



Original Paper

Features and origins of massive dolomite of Lower Ordovician Penglaiba Formation in the northwest Tarim Basin: Evidence from petrography and geochemistry



Zhan-Feng Qiao^{a, b, c, *}, Shao-Nan Zhang^a, An-Jiang Shen^{b, c}, Guan-Ming Shao^{b, c},
Min She^{b, c}, Peng Cao^{b, c}, Xiao-Wei Sun^{b, c}, Jie Zhang^{b, c}, Rui-Xin Guo^a, Xiu-Cheng Tan^a

^a State Key Laboratory of Oil and Gas Reservoir Geology and Exploitation, Southwest Petroleum University, Chengdu, Sichuan 610500, China

^b PetroChina Hangzhou Research Institute of Geology, Hangzhou, Zhejiang 310023, China

^c Key Laboratory of Carbonate Reservoir, China National Petroleum Corporation, Hangzhou, Zhejiang 310023, China

ARTICLE INFO

Article history:

Received 26 July 2020

Accepted 5 March 2021

Available online 4 September 2021

Edited by Jie Hao

Keywords:

Burial dolomite

Dolomitization

Massive dolomite

Lower Ordovician

Penglaiba Formation

Tarim Basin

ABSTRACT

An integrated petrographical and geochemical study of the massive dolomite of the lower Ordovician Penglaiba Formation of the Tarim Basin, outcropping at Yonganba recognized three dolomite types: very finely to finely crystalline nonplanar-a to planar-s dolomite (D1); medium crystalline planar-s to planar-e dolomite (D2); and coarse crystalline nonplanar-a dolomite (D3). All have been affected by burial. D1 and D2 dolomites developed initially before or during shallow burial and later recrystallized, whereas D3 dolomite replaced the initial limestone entirely during burial. All three dolomites have similar geochemical features. The D2 dolomite tends to have more inter-crystalline pores (inherited from primary pores) and higher porosity due to its outstanding compaction resistance during shallow burial; whereas D3 dolomite does not retain appreciable primary pores due to strong cementation and pressure dissolution before dolomitization. This study provides a useful model for understanding the origin and porosity development of burial dolomite, in particular Paleozoic dolomite.

© 2021 The Authors. Publishing services by Elsevier B.V. on behalf of KeAi Communications Co. Ltd. This is an open access article under the CC BY-NC-ND license (<http://creativecommons.org/licenses/by-nc-nd/4.0/>).

1. Introduction

Massive dolomite has an important potential for both hydrocarbon and minerals, and its origin has been an enigma to geologists for centuries, despite a series of models of dolomitization put forward to interpret its ubiquitous occurrence in the stratigraphic record (Adams and Rhodes, 1960; Land, 1980, 1985; Morrow, 1982; Hardie, 1987; Tucker and Wright, 1990; Sun, 1994; Budd, 1997; Machel, 2004; Davies and Smith, 2006). Burial dolomites are sub-surface cements and replacements that form below active phreatic zone reflux and mixing zones in permeable intervals flushed by warm to hot magnesium-enriched basinal and hydrothermal waters (Warren, 2000), and burial dolomitization has been considered as one of the main sources of massive dolomite (Al-Aasm, 2000;

Warren, 2000; Machel, 2004; Carmichael and Ferry, 2008; Ronchi et al., 2011; Conliffe et al., 2012; Azomani et al., 2013; Lapponi et al., 2014; Guo et al., 2016; Dong et al., 2017), besides the pene-contemporaneous dolomitization related to evaporative environments (Folk and Land, 1975; Sun, 1994; Qing et al., 2001; Rott and Qing, 2013).

Numerous researchers have focused on burial dolomitization (Mazzullo, 1992; Reinhold, 1998; Wierzbicki, 2006; Conliffe et al., 2012), including its mechanism and geochemical features. However, it remains difficult to unequivocally interpret the origin of ancient, deeply buried dolomite because of the possible modification during progressive burial, possibly causing recrystallization and chemical alteration (Land, 1980, 1985; Gregg and Shelton, 1990; Al-Aasm, 2000; Al-Aasm and Packard, 2000). Such alteration might make dolomite formed by replacement of precursor limestone especially difficult to successfully distinguish from that formed by recrystallization of former (or contemporaneous) dolomite. For Paleozoic dolomite, this distinction is especially crucial because it potentially dictates porosity development, which is a key

* Corresponding author. State Key Laboratory of Oil and Gas Reservoir Geology and Exploitation, Southwest Petroleum University, Chengdu, Sichuan 610500, China.

E-mail address: qiaozf_hz@petrochina.com.cn (Z.-F. Qiao).

determinant in hydrocarbon reservoir development and exploration.

The Lower Ordovician Penglaiba Formation of the Tarim Basin, Northwest China, consists of dolomite that is more than 200 m thick, consisting mainly of crystalline dolomite intercalated with limestone beds. Lots of researchers have paid attention on the dolomite of Lower Ordovician Penglaiba Formation of the Tarim Basin, and it has been indicated that Penglaiba Formation dolomite has undergone pervasive burial dolomitization (Hu and Jia, 1991; Gu, 2000; Yang et al., 2000; Shao et al., 2002; Zhu et al., 2008; Zhao et al., 2012; Qiao et al., 2012; Zheng et al., 2013), and influenced by tectonic hydrothermal dolomitization related to Permian Magmatic event (Zhu et al. 2009, 2010; Zhang and Luo, 2010; Jiao et al., 2011; Xing et al., 2011; Zhao et al., 2012). However, even though there are some researchers proposed that there are the penecontemporaneous dolomites occurred in Penglaiba Formation (Qian and You, 2006), most of the burial and hydrothermal dolomites were believed to be transferred directly from limestone to dolomite, with fewer consideration of the recrystallization of penecontemporaneous dolomite under the burial or hydrothermal dolomitization (Wu et al., 2008; Zhu et al., 2009), and the criteria to distinguish the limestone-replaced dolomite from the contemporaneous dolomite-recrystallized dolomite keep uncertain, which would be crucial for the evolution and preservation of porosity and, thus, for hydrocarbon reservoir evolution.

Penglaiba Formation dolomite cropping out along the Yonganba outcrop trend in the Bachu area of the northwest Tarim Basin provides an ideal opportunity to investigate the formation of dolomite and burial dolomite. In this paper, we analyze the origin of burial dolomite and analyze the influence of burial dolomitization on porosity. We use a systematic petrographic and geochemical analysis, including X-ray diffraction (XRD), cathodoluminescence, Electron Microprobe and Electron back scattered diffraction image (EBSD) and analysis of carbon and oxygen isotopes, strontium isotopes, and trace elements, to support the sedimentological and petrographic analysis.

2. Geological setting

2.1. Depositional setting and stratigraphy

The Tarim Basin is a large, complex sedimentary basin in Northwest China, with an area of 560,000 km² (Fig. 1a). During the Cambrian and Ordovician periods, it was situated in the southern hemisphere at low latitude close to the South China Platform (Yu et al., 2001). At that time, its west part was a large, stable, shallow marine carbonate platform, on which up to 2000 m of carbonate sediments was deposited (Fig. 1a) (Gu, 2000; Cai et al., 2001; Zheng et al., 2007). The platform was rimmed with microbial buildups during the Cambrian (Gao et al., 2006), and then it transformed into an epeiric platform during the Early Ordovician, as characterized by subtidal–intertidal deposits (Zhu and Ma, 1991), stacking as shallowing-upward cycles.

The Lower Ordovician record of the Tarim Basin includes the Penglaiba Formation and the lower Yingshan Formation, overlaid by the upper Yingshan and Yijianfang Formations of the Middle Ordovician age (Fig. 1b). The Penglaiba Formation features interbedded dolomite and limestone, with the lowermost and uppermost sections dominated by limestone intercalated with dolomite and the middle part mainly dolomite intercalated with sparse limestone (Qiao et al., 2012). The Yingshan Formation features a

dominance of limestone intercalated with dolomite, showing an upward decrease in the proportion of dolomite; the dolomites are mostly scattered, euhedral dolomite rhombs along stylolites in the upper part of the Yingshan Formation (Qiao et al., 2012). The variation in dolomite abundance through this succession reflects, at least in part, basin-wide environmental changes in temperature and seawater chemistry over geologic time (Arvidson and Mackenzie, 1999).

The Yonganba outcrop trend is located at the west margin of the Bachu uplift, which is connected to the central uplift to the east and to the Keping fault-uplift to the northwest (Fig. 1a and c). The Penglaiba Formation in the Bachu uplift region, consistent with those in the Keping and Aksu areas, features interbedded dolomite and limestone, continuous laterally up to 100 km (Qiao et al., 2012). This study focuses on the lower section of the Penglaiba Formation, which consists mainly of dolomite intercalated with sparse limestone (Fig. 1b).

2.2. Burial history and tectonic evolution

The Tarim Basin has undergone multiphase tectonic activity and structural deformation (Kang and Kang, 1994). The burial history for Lower Ordovician successions in the Bachu uplift is illustrated in Fig. 2. Lower Ordovician rocks entered the shallow burial stage soon after deposition and entered the deep burial stage after the Silurian, achieving depths of more than 2000 m. During the Permian, owing to the collision of the middle Tianshan island arc and the Tarim plate, the south Tianshan Ocean closed and the Keping-Bachu uplift formed (Zhang et al., 2001; Ding et al., 2012). Eventually, during the Miocene, strong fold-and-thrust tectonics produced the Kepingtage imbricate thrust belts (Zhang et al., 2001).

3. Materials and methods

A detailed field survey and description of the Penglaiba Formation of the Yonganba outcrop trend in Bachu County were carried out and one section exposed well was measured carefully in order to recognize the sedimentary structure, lithologies, and stacking patterns (Fig. 3a). Additionally, in order to examine the detail petrographic and geochemical features of dolomite, more than 101 plug samples with the length of approximate 10 cm were collected within a window with the area of 10 m × 15 m (Fig. 3b) for thin section production and for geochemistry testing. Next, a careful petrographic and cathodoluminescence examination of thin sections was performed. In order to examine the ordering degree and analyze carbon and oxygen stable isotopes, strontium isotopes, and trace elements and Rare Earth Elements (REE), various types of dolomite were selected. XRD was used to analyze the stoichiometry and, thus, the ordering degree of different types of dolomite. Additionally, Electron Microprobe and Electron back scattered diffraction image (EBSD) were performed on the thin sections of several typical dolomite samples to check the mineral type of inclusions and the variation of element content within the dolomite crystals.

Carbon, oxygen, and strontium isotope measurements were obtained from powders that had been collected from the outcrop plug samples. For stable carbon and oxygen isotopes, about 10 mg of powder was reacted with 100% phosphoric acid for 4 h at 50 °C. The resultant CO₂ was analyzed for oxygen and carbon isotopic ratios on a DELTA V™ Advantage mass spectrometer, as described by Pan et al. (2016). For strontium isotope analysis, 100–150 mg

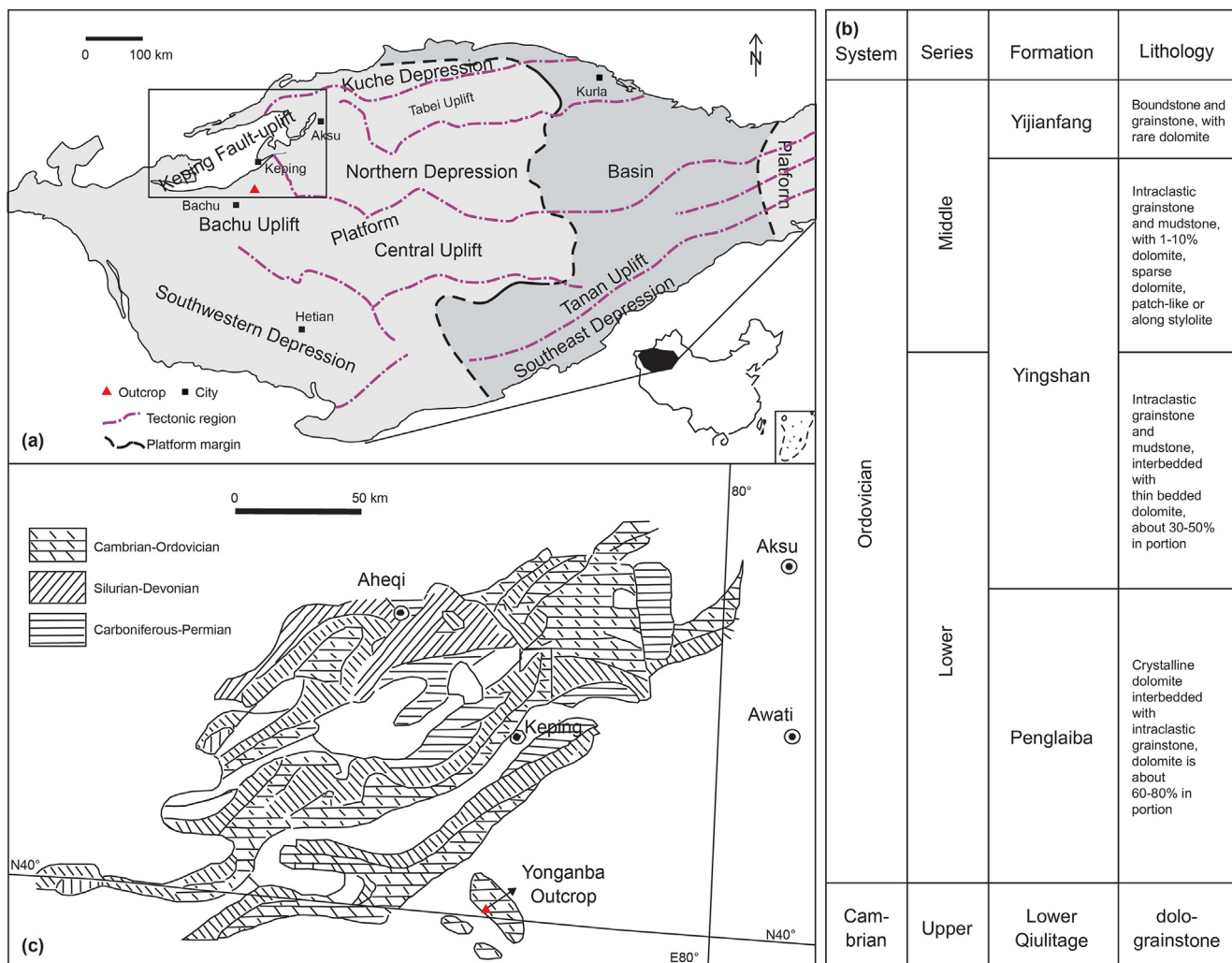


Fig. 1. (a) Regional tectonics of the Tarim Basin and basinal distribution of the Penglaiba Formation. (b) Lower to Middle Ordovician basinal stratigraphy. (c) Geologic map of the study area and the location of the Yonganba outcrop trend.

sample powders were dissolved using a mixture of 1 mL of anhydrous HNO₃ and 1 mL of HF in a crucible at 190 °C for 48 h. Strontium was extracted using conventional exchange procedures (Baadsgard, 1987). The ⁸⁷Sr/⁸⁶Sr ratios were measured on a Triton Plus thermal ionization mass spectrometer and corrected relative to the NBS987 standard, as described by Pan et al. (2016).

Trace elements and REEs were performed on a Thermal X series 2 equipped with a Cetac ASX-510 AutoSampler. Approximately 50 mg of sample powder was digested in Teflon bomb with double distilled concentrated HNO₃–HF (1:4) mixture. The dissolution was maintained on an oven at 185 °C for 3 days. The solutions were then dried down to evaporate HF. The sample residues were re-dissolved with double distilled concentrated HNO₃ followed by 1:1 HNO₃ and dried again. Then, the samples were dissolved in a final 3 mL 2 N HNO₃ stock solution. Finally, sample solution was diluted to 4000 times with 2 percent HNO₃ and added with 10 ppb 61Ni, 6 ppb Rh, In and Re internal spikes. United States Geological Survey (USGS) standard W-2a was used as reference standard and crossed checked with BIR-1, BHVO-2 and other reference materials. Instrument drift mass bias were corrected with internal spikes and external monitors. The ICP-MS procedure for trace element analysis follows the protocol of Eggins et al. (1997) with modifications as described in Kamber et al. (2003) and Li et al. (2005).

All the above experiments were performed in the Key Laboratory of Carbonate Reservoir of China National Petroleum Corporation.

4. Results

4.1. Occurrences of dolomite

The Lower Ordovician dolomite of the Tarim Basin has four types of occurrence: sparse dolomite in limestone, patch dolomite in dolomitic limestone, bedded dolomite, and massive dolomite along faults (Qiao et al., 2012). The Penglaiba Formation in the Bachu area is featured by the bedded dolomite with the thickness of up to 200 m that is overlain and covered by the tight lime grainstone (Fig. 4). In the vicinity of limestone beds, dolomite are interbedded with grainstone layers, and in the upper part of the dolomite section it can be observed that patch limestones are surrounded by dolomite (Fig. 4). Within the dolomite section, crystalline dolomites are intercalated with stromatolitic dolomites and siliceous rocks. Stromatolitic dolomites are mostly located within the bottom of cycles. Siliceous rocks appear as layer or patches and nodules within dolomite, and layered siliceous rock mostly occurs within the range of 30 m to diabase layer, whereas

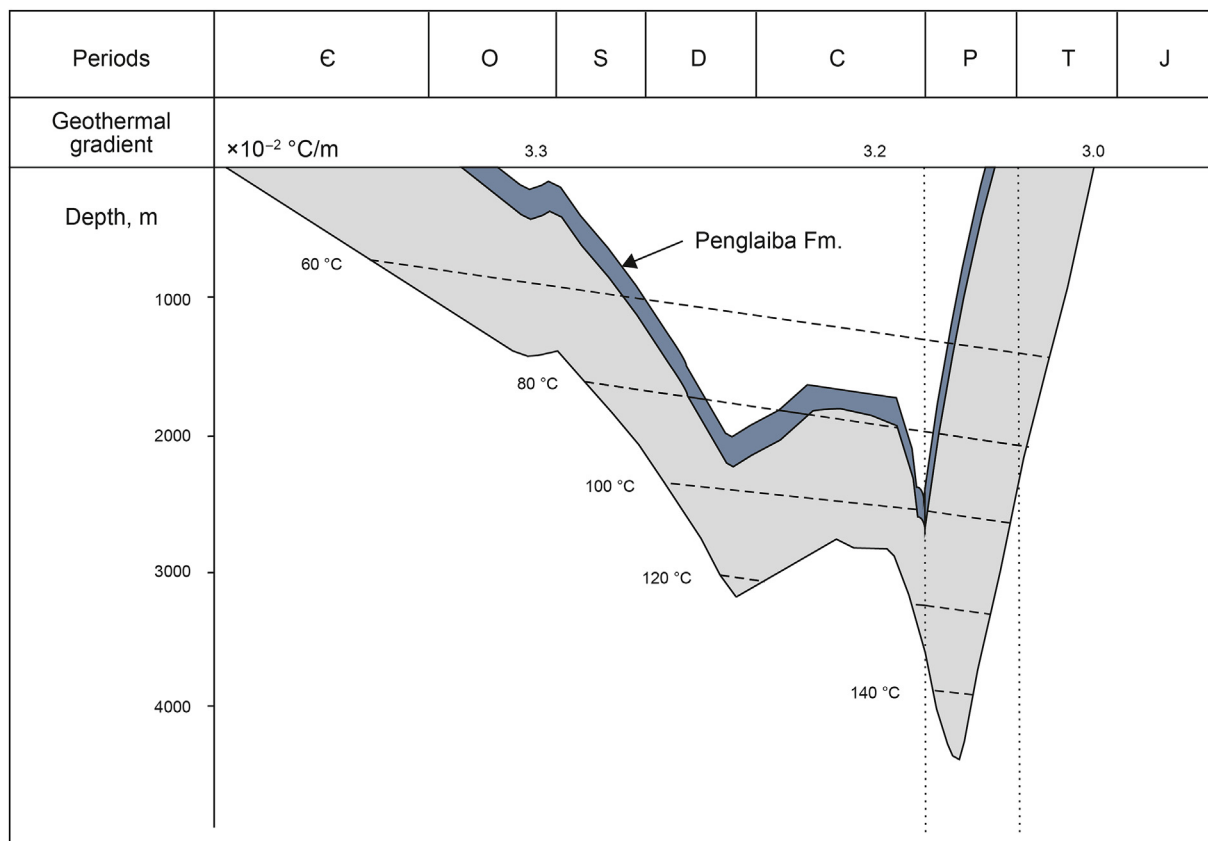


Fig. 2. Burial curve of Lower Ordovician rocks in the northwest Tarim Basin (modified from Hu, 1993).

siliceous patches and nodules cover a wider range.

The focus of this study is on the lower part of the Penglaiba Formation, which is part of the section characterized by thin-bedded, medium, and massive dolomites (Fig. 5a and b). Medium to massive dolomites show cross-bedding, whose thickness varies laterally from 20 to 150 cm (Fig. 5a and c). In these medium to massive dolomites, residual patch-like limestone blocks were observed, with the boundary between limestone and dolomite being ambiguous. This situation clearly differentiates Penglaiba dolomites from those found in classic hydrothermal dolomite. Thin-bedded Penglaiba dolomite is mostly ~10 cm thick (Fig. 5a and d) and is probably related to supratidal environments. Silicification is common in the section as beds and lenticular bodies (Fig. 5a and b).

4.2. Structures of dolomite

Measured section revealed that the dolomites of the Penglaiba Formation include structural types, such as crystalline, algae laminate, and zonal dolomite, also as mentioned in previous researches (Gu, 2000; Wu et al., 2008). The studied window in this paper consists solely of crystalline dolomite, including very finely to finely crystalline dolomite, medium-crystalline dolomite, and coarsely crystalline dolomite, and occasional residual limestone (Fig. 5b).

4.2.1. Very finely to finely crystalline nonplanar-a to planar-s dolomite (D1)

In the outcrop, D1 dolomite shows thin beds and beds of 10 cm thickness (Fig. 5a and c). In thin sections, D1 dolomite crystals, 10–100 μm in size, commonly show nonplanar-a to planar-s

textures (Fig. 6a). Locally, slightly coarse dolomite crystals commonly show a subhedral or petal-like cloudy center surrounded by a clear rim, and the dark fabric seems to be microbial laminae (Fig. 6c). Under cathodoluminescence, D1 dolomite shows dull or nonluminescence with brighter luminescence on the crystal edges (Fig. 6b and d).

4.2.2. Medium-crystalline planar-s to planar-e dolomite (D2)

In the outcrop, D2 dolomite shows cross-beds with thicknesses between 10 and 50 cm (Fig. 5a and c). In thin sections, D2 dolomite crystals, approximately 100–400 μm in size, are present mainly as euhedral to subhedral crystals (planar-s to planar-e textures) (Fig. 7a and b) and show dull or nonluminescence with brighter luminescence on the crystal edges (Fig. 7c), and some samples have multiple zonal features under cathodoluminescence (Fig. 7d). The relatively large crystals generally show a cloudy center surrounded by a clear rim. Ghosts of grains were observed, comprising mosaic D2 associations (Fig. 7a and b). Additionally, stylolites are still recognizable with weak orientation trends evident. Intercrystalline pores are present and are apparently related to grainstone textures (Fig. 7a and b). BESI images revealed that the D2 dolomite has relatively homogeneous crystals with no calcite inclusion (Fig. 7e–i). Siliceous material is observed as dolomite-shape like or patch like (Fig. 7e–i). Some of siliceous material occupies the core of dolomite crystal and has dolomite-like shape and some dolomite inclusions (Fig. 7h and i).

4.2.3. Coarsely crystalline nonplanar-a dolomite (D3)

In the outcrop, D3 dolomites are intercalated with D2 in cross-beds (Fig. 3a and d). In thin sections, dolomite crystals of this type are typically 400–800 μm in size, up to 1500 μm maximum,

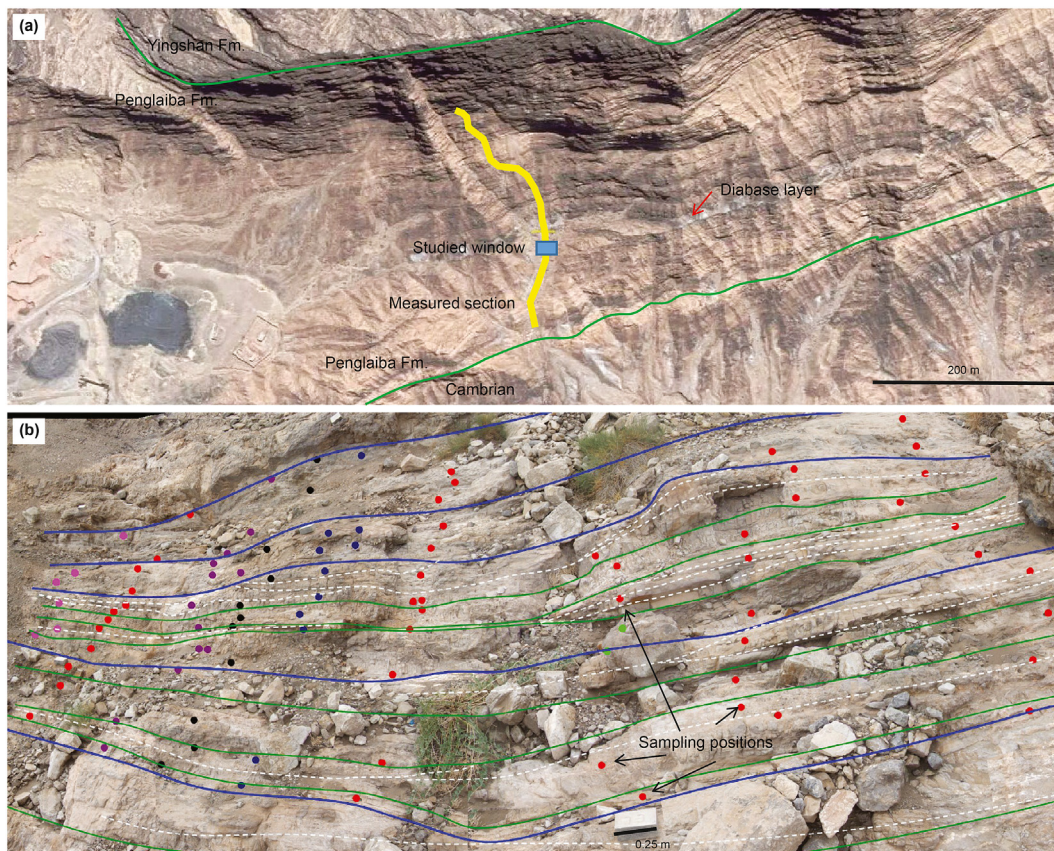


Fig. 3. Photographies showing the studied area and sampling positions. (a) Picture showing the location of measured section and studied window in Penglaiba Fm. The red arrow points to the diabase layer intercalated within the dolomite; (b) Picture showing the sampling positions (colorful spots, different color help to locate the sample position) within the studied window (positions seen in a), note that the dash lines chase the crossbedding boundaries, blue lines show the boundaries of layers.

showing mainly nonplanar-a textures (Fig. 8a and b) and dull or nonluminescence with brighter luminescence on the crystal edges (Fig. 8c). These dolomite crystals commonly show irregularly curved crystal surfaces and appear as mosaic textures with rare intercrystalline pores (Fig. 8a and b). Locally, ghost outlines of precursor particles (mostly peloids) can still be traced under the microscope (Fig. 8a and b). This grainstone texture could be recognized within single D3 crystals (Fig. 8a and b). The incorporation of multiple grainstone ghosts within single D3 crystals is unlike the situation seen in D2 grainstone ghosts. Additionally, some coarsely crystalline D3 dolomites show planar-s to planar-e textures with a cloudy center surrounded by a clear rim. Stylolites were also observed in D3 dolomite. EBSD image and element mapping revealed that, different from the feature of D2 dolomite with rare calcite inclusions, D3 dolomite crystals commonly host lots of calcite inclusions, which happened randomly within anywhere of the crystal (Fig. 8d–f). Calcite inclusion has irregular shape and could be up to 80 μm (Fig. 8d–f), and it seems that those larger inclusions tend to occur along the crystal edges but not be constrained by the boundary of the crystal (Fig. 8d–f). Additionally, quartz inclusions were observed within the bright edges of D3 dolomite (Fig. 8g).

4.2.4. Grainstone (L) with coarsely crystalline dolomite (D4)

In the outcrop, L grainstones are cross-bedded or massive with bed thicknesses of 0.5–1.5 m. In thin sections, L grainstone shows a classic grainstone texture, consisting of intraclasts or peloids mostly cemented tightly by two-generation calcites (Fig. 8h and i). The tight grainstone cementation keeps these regions

undolomitized, situated directly within D3 dolomite beds, either with ambiguous boundaries or interbedded with dolomites. Coarse but irregular dolomite crystals (D4) occur between particles or along stylolites (Fig. 8h and i); in some cases, such dolomites are seen replacing other crystals in a fabric-destructive way (Fig. 8h and i). D4 dolomite shows cathodoluminescence features similar to those of D3 dolomite (Fig. 8j).

Quartz cements were observed frequently, either partially or completely filling vugs, fractures, and intercrystalline pores. In thin sections, quartz cements immediately envelop dolomites, on which corrosive microreliefs may be locally present. Volumetrically, these quartz cements are of minor importance, making up less than 2% of the rocks.

Chert nodules and layered cherts were intercalated within dolomite in the studied section (Fig. 3a). Thin section observation revealed that precursor textures were preserved within chert nodules and layered cherts.

4.3. Geochemistry results

4.3.1. Ordering degree by XRD and element composition by EP

A wide range of ordering degrees is displayed across the different dolomite types. D1 dolomite generally shows ordering degrees from 0.62 to 0.85, with an average of 0.74 (Table 1, Fig. 9a). D2 dolomite shows generally higher ordering degrees compared to D1 dolomite, ranging from 0.70 to 0.89, with an average of 0.81 (Table 1, Fig. 9a). The ordering degree of D3 dolomite varies widely from 0.45 to 0.98, with an average of 0.76 (Table 1, Fig. 9a).

EBSD and element composition by EP indicate that D3 dolomite

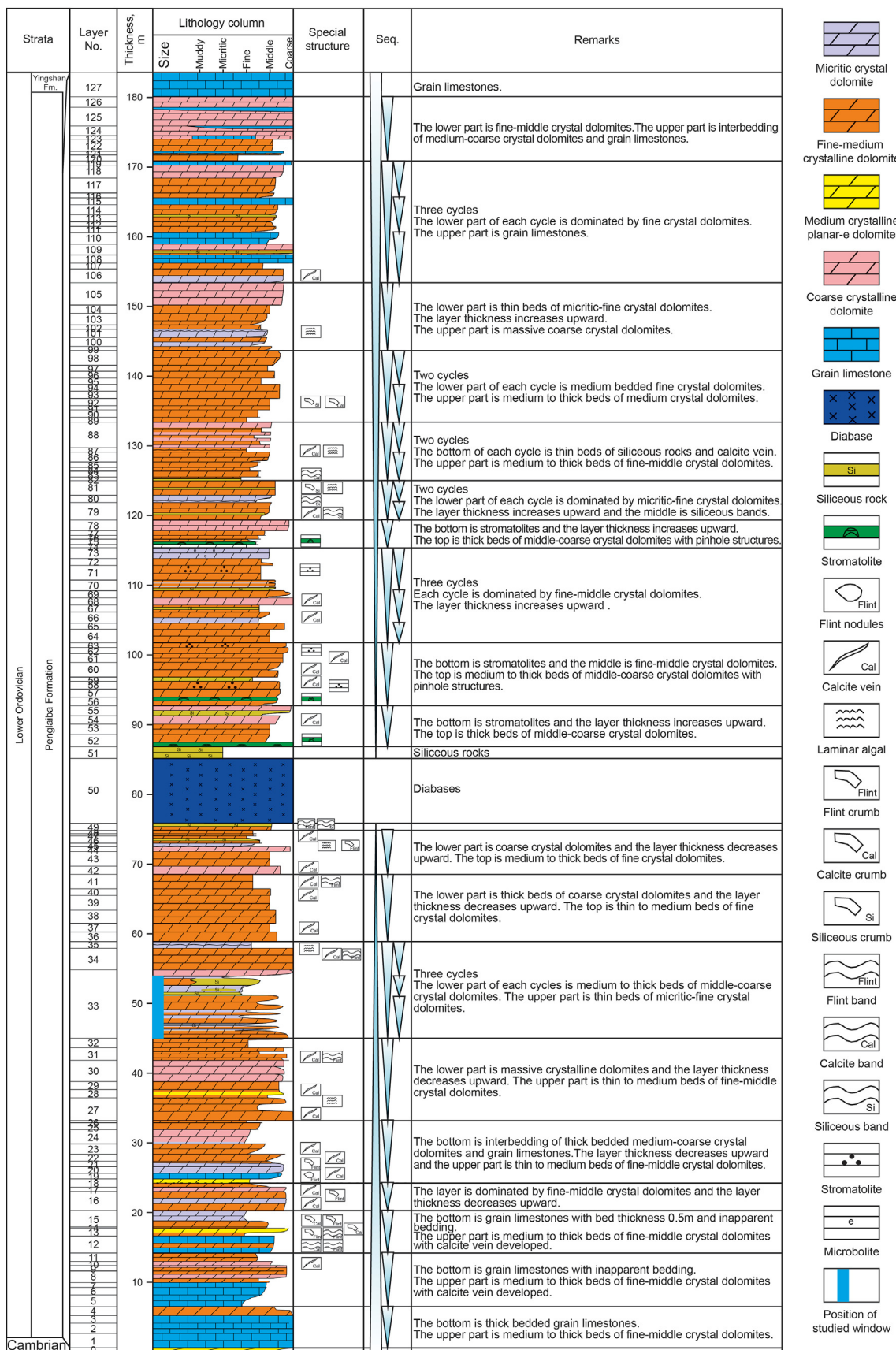


Fig. 4. The column of dolomite section of Penglaiba Formation of Yonganba Outcrop (Blue line in lithology column showing the position of studied window).

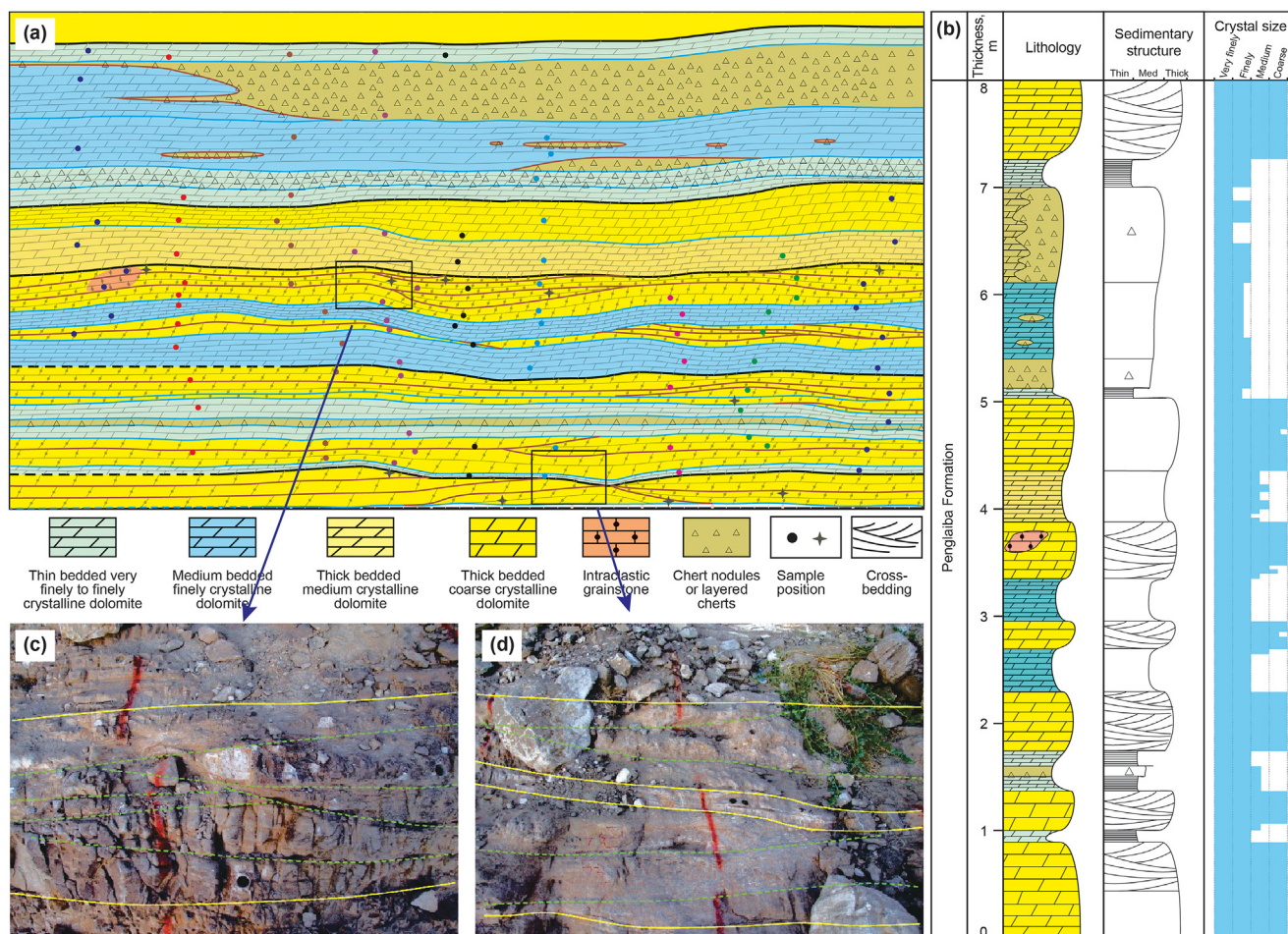


Fig. 5. Features of the study outcrop. (a) A 2D sketch showing the studied window with lithology and sample positions. (b) Stratigraphic column of the study section showing sedimentary structures and crystal size profile, position in Penglaiba Formation seen in Fig. 4. (c) Photo of thick-bedded, medium-crystalline dolomite with cross-bedding. (d) Photo of outcrop showing thin-bedded, finely crystalline dolomite intercalated with thick-bedded, coarsely crystalline dolomites.

has complicated structure and element composition, including calcite and quartz inclusions and various Mg/Ca ratio from 0.728 to 1.073 (Table 2). Calcite inclusions in edges of D3 dolomite seem have higher Na and K contents and less Sr than those in the cores of D3 dolomite.

4.3.2. Mn and Sr contents by ICP-MS

Different types of dolomite show different ranges of Mn and Sr contents (Fig. 9b). D1 dolomite generally shows Mn contents ranging from 34.2 to 78.3 $\mu\text{g/g}$, with an average of 62.6 $\mu\text{g/g}$. As for Sr, D1 dolomite generally shows Sr contents ranging from 61.0 to 121.3 $\mu\text{g/g}$, with an average of 111.7 $\mu\text{g/g}$ (Table 1, Fig. 9b). D2 dolomite yields Mn contents ranging from 64.2 to 103.6 $\mu\text{g/g}$, with an average of 78.0 $\mu\text{g/g}$. As for Sr, D2 dolomite yields Sr contents ranging from 31.4 to 87.1 $\mu\text{g/g}$, with an average of 50.8 $\mu\text{g/g}$ (Table 1, Fig. 9b). In short, D1 dolomites show generally lower Mn and higher Sr contents compared to D2 dolomites. The Mn and Sr contents of dolomites tend to show a negative correlation (i.e., with the decrease of the Sr content, the Mn content increases) (Table 1, Fig. 9b).

D3 dolomite shows a wider range of Mn and Sr contents. The Mn content in D3 dolomite varies from 22.1 to 114.0 $\mu\text{g/g}$, with an average of 57.3 $\mu\text{g/g}$. The Sr content in D3 dolomite varies from 42.6 to 191.9 $\mu\text{g/g}$, with an average of 85.7 $\mu\text{g/g}$ (Table 1, Fig. 9b).

4.3.3. Oxygen and carbon stable isotopes

D1 dolomite yields $\delta^{13}\text{C}$ values ranging from -1.289‰ to -2.875‰ VPDB, with an average of -1.864‰ . As for oxygen, D1 dolomite yields $\delta^{18}\text{O}$ values ranging from -6.080‰ to -7.757‰ VPDB, with an average of -7.315‰ (Table 1, Fig. 9c). D2 dolomite generally shows $\delta^{13}\text{C}$ values ranging from -0.471‰ to -1.902‰ , with an average of -1.194‰ . As for oxygen, D2 dolomite generally shows $\delta^{18}\text{O}$ values ranging from -5.988‰ to -8.456‰ VPDB, with an average of -7.208‰ (Table 1, Fig. 9c). For D3 dolomite, the $\delta^{13}\text{C}$ values vary from -0.013‰ to -2.909‰ VPDB, with an average of -1.362‰ , and the $\delta^{18}\text{O}$ values vary from -5.524‰ to -12.810‰ VPDB, with an average of -8.649‰ (Table 1, Fig. 9c). Overlaps between different dolomites are substantial for $\delta^{13}\text{C}$ and $\delta^{18}\text{O}$ values. The $\delta^{18}\text{O}$ values of D1 and D2 dolomites are distributed in a similar range, with similar average values (Table 1, Fig. 9c). D3 dolomite shows a wider range of $\delta^{18}\text{O}$ values, but almost all of these values fall within the respective estimated isotopic ranges of calcite precipitated from late Cambrian–Early Ordovician seawater (Qing and Veizer, 1994; Veizer et al., 1999; Shields et al., 2003): -11.1‰ to -6.0‰ VPDB for $\delta^{18}\text{O}$ and -3.0‰ to 0‰ VPDB for $\delta^{13}\text{C}$. The only exceptions are two D3 dolomite samples yielding $\delta^{18}\text{O}$ values as extreme as -13.0‰ VPDB.

4.3.4. $^{87}\text{Sr}/^{86}\text{Sr}$ ratio

D1 dolomite yields $^{87}\text{Sr}/^{86}\text{Sr}$ ratios ranging from 0.709152 to

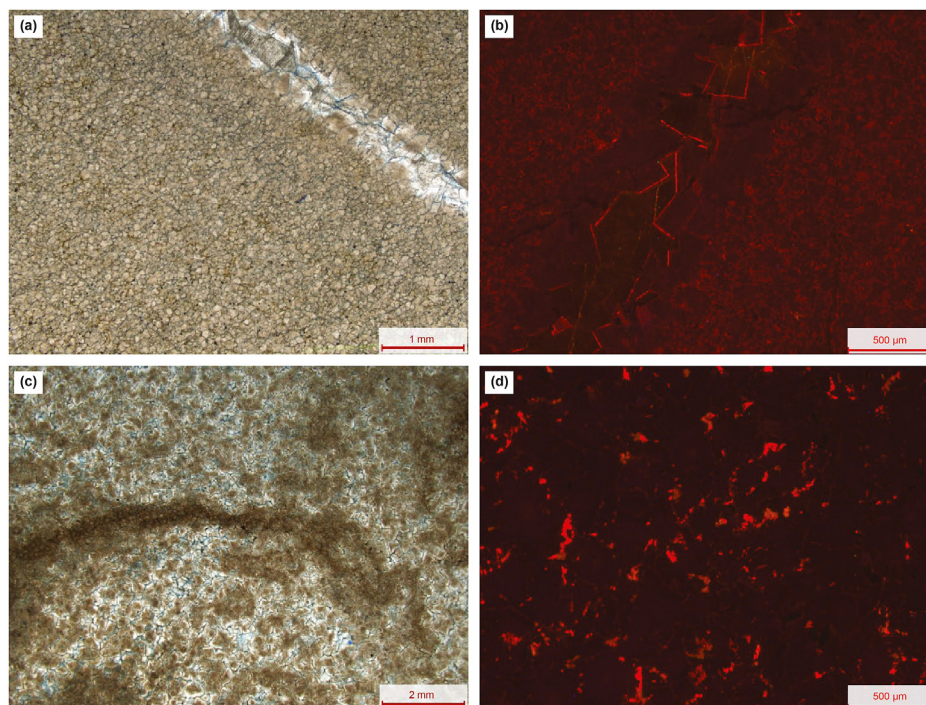


Fig. 6. Micrograph and cathodoluminescence images of very finely to finely crystalline dolomite (D1). (a) Microscope photo showing very finely crystalline dolomite with fractures filled with zonal dolomite. (b) Cathodoluminescence photo of the sample shown in (a) showing dull or nonluminescence features and bright luminescent edges of dolomite filled within a fracture. (c) Micrograph showing finely crystalline dolomite with a cloudy center and probable microbial laminae. (d) Cathodoluminescence image of the sample shown in (c) showing dull or nonluminescence features and orange luminescence around the crystal edges.

0.709308, with an average of 0.7092084 (Table 1, Fig. 9d). D2 dolomite yields $^{87}\text{Sr}/^{86}\text{Sr}$ ratios ranging from 0.708825 to 0.710198, with an average of 0.7095883, clearly higher than that of D1 dolomite (Table 1, Fig. 9d). The $^{87}\text{Sr}/^{86}\text{Sr}$ ratios of D3 dolomite show a wider range, from 0.708957 to 0.709786, with an average of 0.7093717 (Table 1, Fig. 9d). Most samples show $^{87}\text{Sr}/^{86}\text{Sr}$ ratios higher than the estimated value of contemporaneous seawater: 0.7085–0.7091 (Fig. 9d) (Qing et al., 1998; Wadleigh and Veizer, 1992).

4.3.5. Rare Earth Elements (REEs)

The REE patterns and abundances in dolomites and limestone are very similar with enriched LREE (Light REE), and comparably D1 dolomites seem have relatively higher and narrower range of HREE (Heavy REE) (Table 3, Fig. 10), and three types of dolomites have comparable mean values of total REE (ΣREE contents of 4.398 $\mu\text{g}/\text{g}$ for D1 dolomite, 3.178 $\mu\text{g}/\text{g}$ for D2 dolomite, and 4.448 $\mu\text{g}/\text{g}$ for D3 dolomite).

5. Discussion

5.1. Paragenesis and dolomitization stages

5.1.1. Paragenesis

Burial history and petrography features revealed that the Penglaiba Formation experienced at least three stages of diagenetic modification (Fig. 11), including penecontemporaneous stage, burial dolomitization stage, and post dolomitization stage.

Penecontemporaneous stage is featured by the compaction and rimmed cements surrounding the intraclasts (Fig. 8g, h). The stylolite-like contact and the absence of rimmed cements between some of the particles revealed that the compaction happened pretty early (Fig. 8i), and the fact that the compaction modified the

rimmed cements suggests they both happened during penecontemporaneous stage (Fig. 8h).

During burial stage, many kinds of diagenesis occurred, including cementation, dolomitization, stylolite, fracturing, and silicification, and the relation between the dolomite and stylolite and fracture suggests at least three generation of stylolite and three generation of fracturing (Fig. 11). During shallow burial stage of late Ordovician to Silurian, with the increase of pressure and temperature, first generation of stylolite started forming, and correspondingly, second generation cementation in grain limestone happened and the cements filled most of the spaces between the particles, which is a crucial diagenesis for the destruction of intergranular porosity. During this stage, it is observed that the stylolite was modified by dolomitization with only ambiguous shape left in some cases (Fig. 12a). The second generation of stylolite featured by the stylolite-like contact of D3 dolomite crystals and cut the D2 dolomite (Fig. 12b), occurred probably during late Devonian to early Carboniferous Hercynian uplift, corresponding the fractures cut the D2 and D3 dolomite with dolomite filled. All the dolomite fabrics were cut by silicification, calcite veins, and third generation of stylolite (Fig. 12c), and the close relationship of silicification with the diabase layer suggest that stylolite and silicification occurred during Permian when the volcanic province formed.

5.1.2. Dolomitization stages

Middle Ordovician scattered, euhedral dolomite rhombs along stylolites grade into pervasive, dense, interlocking mosaics of anhedral Lower Ordovician dolomite typical for dolomites formed during burial diagenesis. Furthermore, the paragenesis frame constrains at least three dolomitization stages, including penecontemporaneous, shallow burial, and Hercynian tectonic related dolomitization.

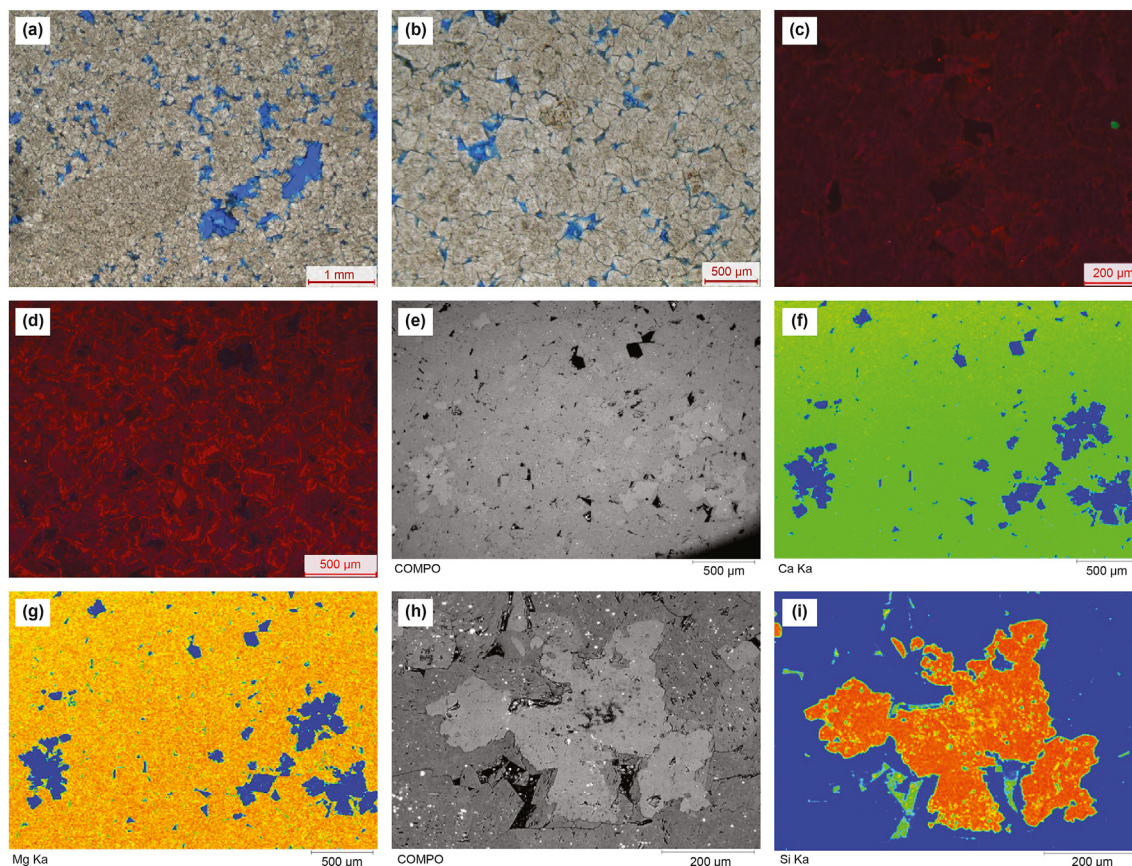


Fig. 7. Micrographs, cathodoluminescence, and EBSD images of medium-crystalline dolomite (D2). (a) Micrograph showing features of planar-s to planar-e D2 dolomite with residual grainstone fabric and intergranular porosities; (b) micrograph showing the arrangement of dolomite crystals controlled by primary grainstone fabric and intercrystalline pores converted from intergranular pores; (c) cathodoluminescence image of sample shown in (b) showing dull or non-luminescence features of dolomite and bright luminescence around the crystal edges; (d) cathodoluminescence image of D2 dolomite showing zonal luminescence features; (e) EBSD micrograph of D2 dolomite showing the homogeneous dolomite crystals with quartz and intercrystalline pores; (f) Ca element mapping of sample shown in (e) showing homogeneous structure within the dolomite; (g) Mg element mapping of sample shown in (e) showing homogeneous structure within the dolomite; (h) EBSD micrograph of D2 dolomite showing the quartz replaced the dolomite, with some dolomite inclusions within quartz; (i) Si element mapping of sample shown in (h) showing the quartz replaced the dolomite, with some dolomite inclusions within quartz.

Penecontemporaneous dolomitization is believed occurred, based on the observation that D1 dolomite recrystallized and fracture filling dolomite simultaneously (Fig. 6a), which points to the sequence of penecontemporaneous dolomitization, fracturing, and dolomite recrystallization. Additionally, the fine crystalline, fabric-retentive nature and dull cathodoluminescence suggest early dolomitization of marine lime mud at near-surface conditions prior to significant compaction, similar to the case for Lower Ordovician dolomites of eastern Laurentia (Azomani et al., 2013).

Shallow burial dolomitization is featured by the close relation of dolomite and stylolite. The fact that the D2 dolomite modified the stylolite (Fig. 12a) and D3 and D4 dolomite distributed along the stylolites (Fig. 8g) suggests that the dolomitization occurred during burial stage, which is consistent with the Mazzullo's (1992) statement that nonplanar textures (D3 dolomite) developed most commonly in the burial environment above the CRT (Critical Roughening Temperature, about 60 °C according to Gregg and Shelton (1990)). Additionally, the preservation of intergranular porosity and residual grainstone fabric in D2 dolomite probably revealed that the penecontemporaneous dolomitization occurred before the rock is buried too deep to form pervasive stylolite and prevent from the significant cementation, and the zonal feature of D2 dolomite crystals and crosscut with stylolite suggest they recrystallized during shallow burial environment (Fig. 12a, b).

The D4 dolomites in grainstone mostly follow stylolites or

expand from intergranular pores (Fig. 8g, h, i) proved that they formed in burial environment, meanwhile or shortly later than the period of D2 formed, and the similarity of cathodoluminescence features of D3 dolomite and D4 dolomite suggest the consistency of their origins, and the features of grainstone fabric in single D3 dolomite crystal and tightly cemented residual grainstone patches within D3 dolomite beds imply that the dolomitization for D3 dolomite occurred after mineral stabilization and was fabric-destructive. Additionally, the mosaic or stylolite-like contact of D3 dolomite suggest the following compaction probably during early Hercynian tectonic movement of late Devonian to early Carboniferous. Permian volcanic activity related silicification and fracturing constrain that all the dolomite formed before them.

5.2. Geochemistry and dolomitization fluids

5.2.1. Ordering degree and major and trace elements

Ordering degrees, as examined by XRD, could be used to analyze the crystal features of dolomite. Ordering degrees higher than 0.8, as seen in D2 dolomite and some D3 dolomite, typically indicate near-stoichiometric dolomite (Fig. 9a). Some D3 dolomite shows ordering degrees lower than 0.8, pointing to an Mg ion deficit and a less stoichiometric dolomite (Fig. 9a). This situation is typically interpreted as a result of partial dolomitization. In this scenario, the dolomite contains more calcite inclusions (Machel, 2004); the

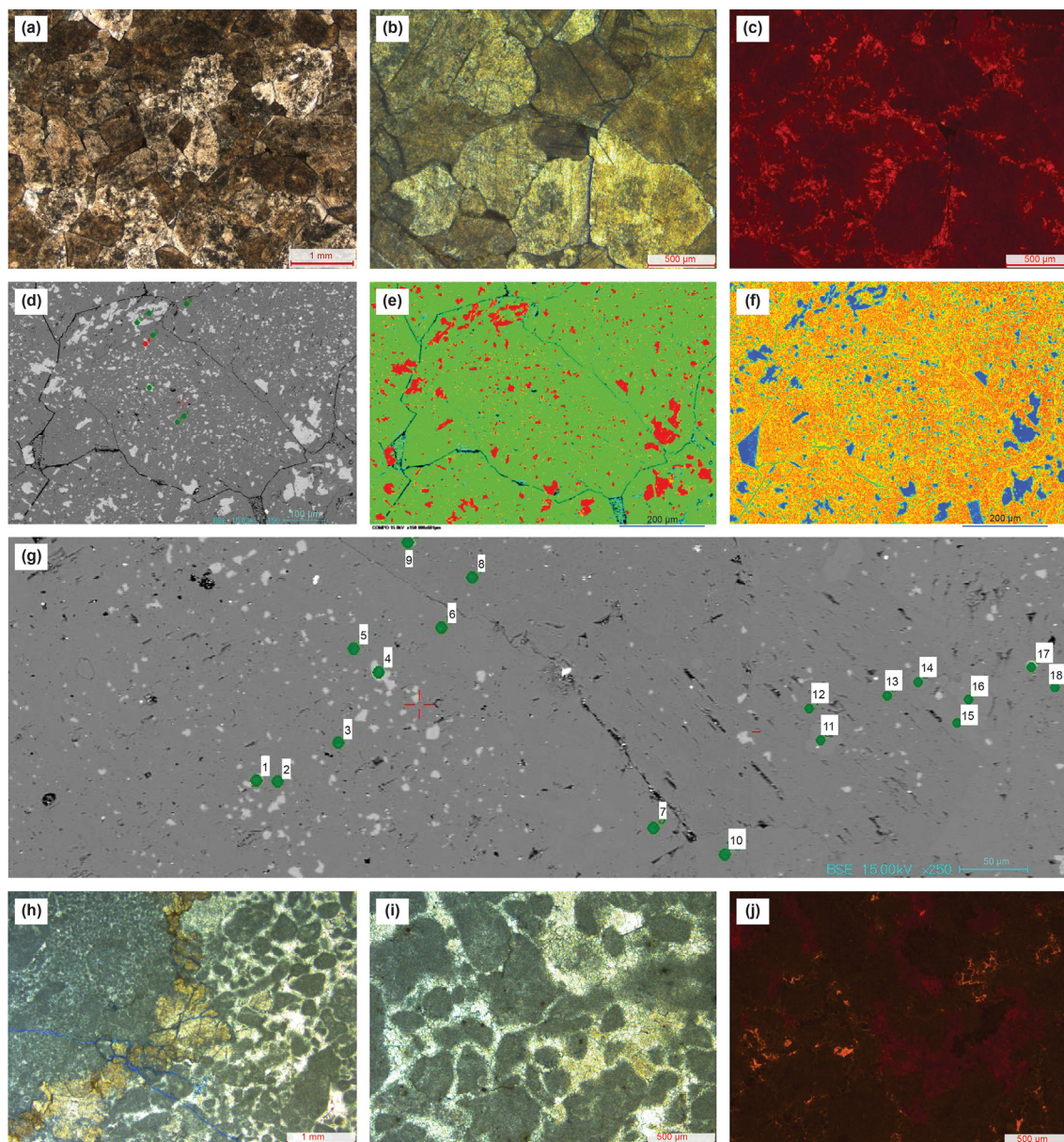


Fig. 8. Micrographs, cathodoluminescence, and EBSD images of coarsely crystalline dolomite (D3) and dolomite patch (D4) in grainstone. (a) Micrograph showing D3 with planar textures and grainstone fabric within single dolomite crystal; (b) Micrograph showing D3 with mosaic contact and brighter edges; (c) Cathodoluminescence photo of (b) showing dull luminescence features of D3 dolomite cores and orange luminescence features of D3 dolomite edges, note that the boundaries between dull cores and orange edges are irregular. (d) BESI Micrograph showing the irregular D3 dolomite crystals with lots of calcite inclusions (white spots), and calcite inclusion seems uncontrolled by crystals; (e) Ca element mapping by EP showing the distribution of calcite inclusions (red color); (f) Mg element mapping by EP showing the heterogeneous dolomite structure due to the calcite inclusions (blue to green color). (g) BESI micrograph showing the internal structure of D3 dolomite cores and edges, note that zonal structure and quartz inclusions are observed in edges, with less calcite inclusions than the core of dolomite, green spots point the location of EP analysis. (h) Micrograph showing the D4 dolomite occurred along the stylolite, with grainstone cemented tightly. (i) Micrograph showing D3 grainstone cemented tightly and coarse but irregular dolomite crystals (D4) occurring between D3 particles, replacing the grainstone gradually. (j) Cathodoluminescence image of the sample shown in i showing dull luminescence features of D4 dolomite and nonluminescence features of D4 grainstone.

degree of measured cation order increases with the percentage of dolomite despite a dolomite composition remains relatively constant. Additionally, D1 dolomites show relatively low ordering degrees (<0.8), implying Sabkha-like dolomitization, which is consistent with the observed petrographic features.

The Sr and Mn concentrations in carbonate are controlled by distribution coefficients (Banner, 1995), with normal seawater precipitating Sr-enriched and Mn-depleted calcite (or aragonite). The distribution coefficient of Sr in dolomite is less than 1 (0.039–0.048, Banner, 1995) and only half the value of the Sr

distribution coefficient in calcite (Vahrenkamp and Swart, 1990; Banner, 1995), whereas the distribution coefficient of Mn in dolomite is higher than 1 (Vahrenkamp and Swart, 1990). Consequently, more Sr cations tend to stay in the diagenetic fluid, whereas more Mn cations tend to enter the crystal lattice during the dolomite replacement of calcite and the recrystallization of dolomitization (Banner, 1995; Huang et al., 2006). These patterns together produce the negative correlations across dolomites (here, the D1 and D2 dolomites) of Sr and Mn (Fig. 9b) and of Sr and the ordering degree (Fig. 13a). Additionally, diagenetic reactions mediated by marine

Table 1
Geochemical data for different dolomites of the Penglaiba Formation.

No.	Dolomite	Ordering degree	Mn, $\mu\text{g/g}$	Sr, $\mu\text{g/g}$	$\delta^{13}\text{C}$, PDB‰	$\delta^{18}\text{O}$, PDB‰	$^{87}\text{Sr}/^{86}\text{Sr}$
YAB-1	D1	0.85	54.1	70.2	-2.875	-7.570	0.709308
YAB-2	D1	0.71	78.3	108.1	-1.819	-7.757	0.709196
YAB-3	D1	0.72	77.1	121.3	-1.471	-6.080	0.709165
YAB-4	D1	0.62	34.2	197.7	-1.289	-7.851	0.709152
YAB-5	D1	0.81	69.5	61.0	—	—	0.709221
YAB-6	D2	0.70	60.7	82.6	—	—	0.708825
YAB-7	D2	0.77	76.6	87.1	-0.649	-5.988	0.709409
YAB-8	D2	0.84	103.6	31.4	-1.131	-7.396	0.709771
YAB-9	D2	0.80	72.5	38.3	-0.471	-6.423	0.709892
YAB-10	D2	0.84	86.6	43.7	-1.902	-8.456	0.710198
YAB-11	D2	0.84	74.1	35.1	—	—	0.70959
YAB-12	D2	0.89	71.7	37.7	-1.818	-7.777	0.709433
YAB-13	D3	0.88	64.2	93.1	—	—	0.709467
YAB-14	D3	0.76	67.8	57.9	—	—	0.709566
YAB-15	D3	0.80	114.0	77.7	—	—	0.709565
YAB-16	D3	0.76	67.1	58.8	-1.519	-7.845	0.709162
YAB-17	D3	0.98	62.4	42.6	-1.119	-7.927	0.709239
YAB-18	D3	0.83	80.8	58.0	—	—	0.709786
YAB-19	D3	0.82	78.4	50.2	—	—	0.709455
YAB-20	D3	0.84	74.3	62.5	-1.209	-8.458	0.709661
YAB-21	D3	0.81	83.4	51.4	-0.575	-8.131	0.709422
YAB-22	D3	0.80	83.8	80.7	-0.460	-8.539	0.70927
YAB-23	D3	0.80	52.8	152.6	-2.909	-8.351	0.709327
YAB-24	D3	0.83	76.6	81.3	-1.598	-8.268	0.709329
YAB-25	D3	0.96	67.3	52.3	-1.083	-9.260	0.709265
YAB-26	D3	0.78	34.6	108.7	-2.199	-8.165	0.709183
YAB-27	D3	0.69	31.8	75.4	-1.587	-12.810	0.709525
YAB-28	D3	0.71	22.1	105.7	-0.990	-6.910	—
YAB-29	D3	0.73	33.1	56.7	-1.194	-8.236	0.709325
YAB-30	D3	0.45	26.7	191.9	-1.901	-5.524	0.708957
YAB-31	D3	0.74	42.8	74.1	-0.967	-8.599	0.709563
YAB-32	D3	0.62	25.4	56.5	-1.118	-8.394	0.709207
YAB-33	D3	0.59	47.8	139.8	0.013	-8.859	0.709322
YAB-34	D3	0.64	23.2	158.5	-2.735	-12.751	0.709210

pore waters may alter the Sr/Ca and Mg/Ca ratios of the fluids involved in dolomitization (Baker and Burns, 1985; Kimbell and Humphrey, 1994; Banner, 1995), during replacement and/or recrystallization in the burial stage, the Sr concentration in dolomite or calcite tends to decrease, whereas the Sr concentration in diagenetic fluids tends to increase, so more Sr cations have the opportunity to enter the crystal lattice for late-formed dolomite (Banner, 1995). This probably explains the wide range of Sr and Mn distributions despite their distinct correlation. In contrast, the wider range of Sr and Mn contents in D3 dolomite of low ordering degree is attributed to the residual calcite composition or to calcite inclusions in D3 dolomite, as well as to potentially varied Sr concentrations in diagenetic fluids. The pattern of high Sr and low Mn concentrations in D1 dolomite is also consistent with the interpretation of penecontemporaneous dolomitization.

5.2.2. C, O, and Sr isotopes and REE

C and O isotopes of all types of dolomite, in spite of their wide range, fall within the estimated isotopic ranges for calcites precipitated from late Cambrian–Early Ordovician seawater (Qing and Veizer, 1994; Veizer et al., 1999; Shields et al., 2003): -11.1‰ to -6‰ VPDB for $\delta^{18}\text{O}$ and -3.0‰ to 0‰ VPDB for $\delta^{13}\text{C}$. The relatively negative $\delta^{18}\text{O}$ of D3 dolomite than D1 and D2 dolomite probably resulted as the dolomitization in later and deeper burial environment, as proposed in the Monterey Formation of California by Malone et al. (2010) that the variation in the $\delta^{18}\text{O}$ compositions of the dolomites is the result of their more extensive recrystallization at the higher temperatures during burial. On the other hand, all types of dolomite show $^{87}\text{Sr}/^{86}\text{Sr}$ ratios higher than the value of contemporaneous seawater: 0.7085–0.7091 (Wadleigh and Veizer, 1992; Qing et al., 1998). Unlike trace elements and stable C and O

isotopes, Sr isotope compositions of carbonate minerals directly record fluid isotope compositions (Banner, 1995). A comparison of the ordering degrees, Sr contents, oxygen isotopes, and $^{87}\text{Sr}/^{86}\text{Sr}$ ratios shows that the Sr content decreases (Fig. 13a) and $^{87}\text{Sr}/^{86}\text{Sr}$ ratios increase (Fig. 13b) with increasing ordering degree of dolomite, whereas the $^{87}\text{Sr}/^{86}\text{Sr}$ ratios increase with decreasing Sr content (Fig. 13c) and with the depletion of oxygen isotopes (Fig. 13d). The good correlation of the Sr content, oxygen isotopes, $^{87}\text{Sr}/^{86}\text{Sr}$ ratios, and ordering degrees is interpreted as related substantially to water–rock interaction (i.e., replacement or recrystallization of dolomite) in a burial environment (Sibley and Gregg, 1987; Reinhold, 1998; Montanez and Read, 1991).

Huang et al. (2006) noted that the $^{87}\text{Sr}/^{86}\text{Sr}$ ratios in dolomite in the Feixianguan Formation of the northeast Sichuan Basin increased above contemporaneous seawater values and increased with decreasing Sr content, and they attributed this pattern to contamination of the system by allochthonous radioactive Sr. Azmy et al. (2001) noted that the $^{87}\text{Sr}/^{86}\text{Sr}$ ratios in pre-Cambrian dolomites of the São Francisco Basin clearly increased above contemporaneous seawater values at a relatively high homogeneous temperature, and again they interpreted this pattern as a result of radioactive Sr brought in by dolomitizing fluid circulated from underlying clastic formations. However, the Penglaiba Formation dolomites' distinct correlation of ordering degree, Sr and Mn contents, and $^{87}\text{Sr}/^{86}\text{Sr}$ ratios across different dolomite types points to seawater-derived dolomitizing fluid, as presented by Zhang et al. (2008). Indeed, the fluid that drives the formation of replacement dolomite normally is either seawater or seawater-derived fluid (Land, 1985; Hardie, 1987; Budd, 1997). Notably, some researchers have reported past hydrothermal activity in the study area (Sun et al., 2007; Zhu et al. 2009, 2010; Zhang and Luo, 2010; Jiao

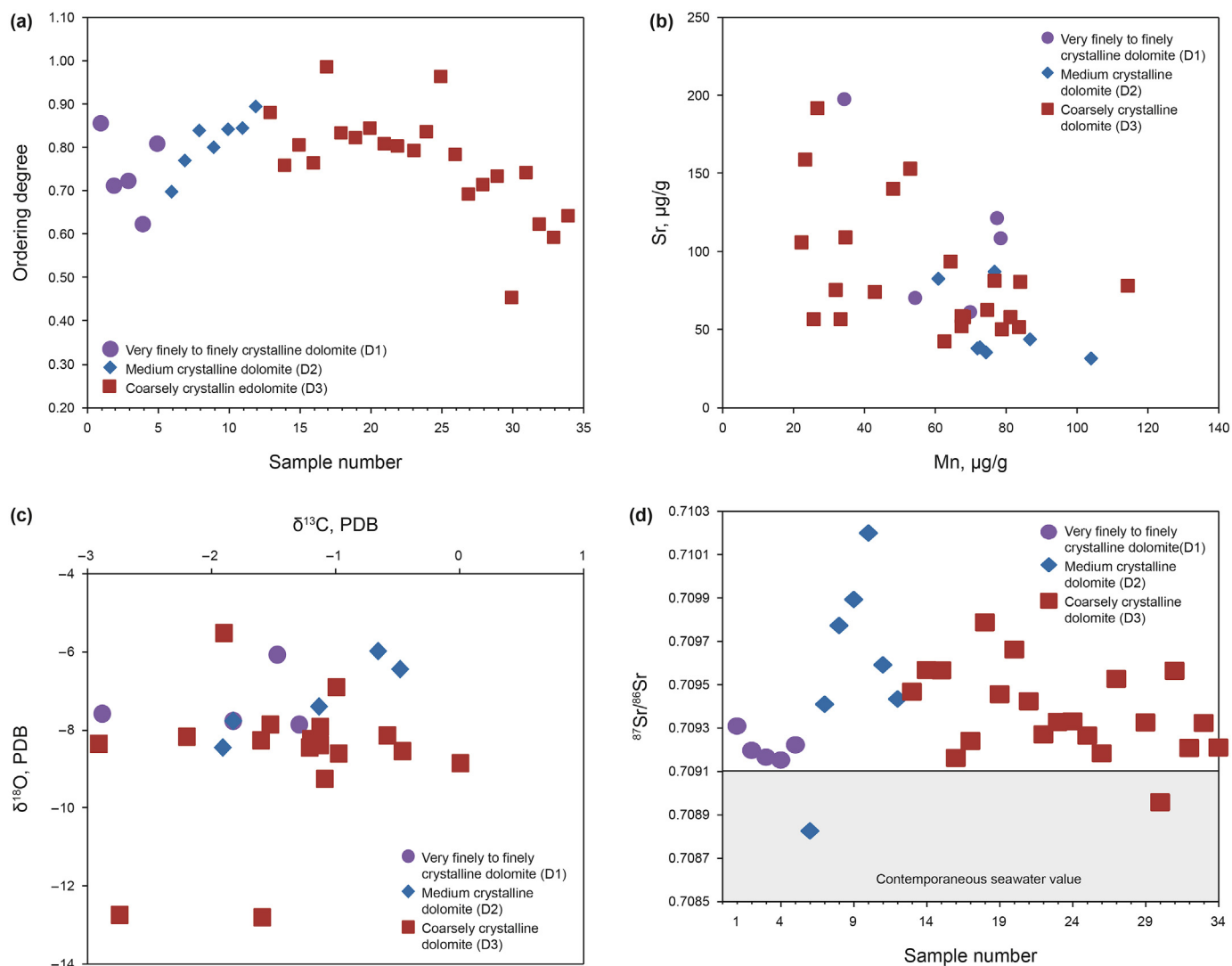


Fig. 9. Geochemistry of various Penglaiba Formation dolomites. (a) Ordering degree of various dolomites. (b) Sr and Mn contents of various dolomites. (c) $\delta^{18}\text{O}$ and $\delta^{13}\text{C}$ of various dolomites. (d) $^{87}\text{Sr}/^{86}\text{Sr}$ ratios of various dolomites.

Table 2
Element composition of dolomite and inclusions by Electron Probe (point positions in Fig. 8g).

Analyzed points	Mg, mol%	Ca, mol%	Mg/Ca	MgO	CaO	Na ₂ O	K ₂ O	Al ₂ O ₃	SiO ₂	P ₂ O ₅	SO ₃	TiO ₂	MnO	FeO	ZnO	SrO	BaO	total
1	0.894	98.065	0.009	0.348	53.193	0.274	0.024	0.000	0.000	0.022	0.000	0.151	0.000	0.098	0.000	0.155	0.000	54.265
2	51.222	48.516	1.056	24.317	32.047	0.000	0.012	0.000	0.000	0.000	0.000	0.000	0.000	0.000	0.000	0.000	0.000	56.376
3	51.287	48.453	1.058	24.133	31.722	0.000	0.000	0.000	0.071	0.000	0.050	0.000	0.000	0.024	0.000	0.000	0.000	56.000
4	2.428	97.246	0.025	0.995	55.423	0.067	0.000	0.000	0.000	0.000	0.000	0.000	0.000	0.000	0.000	0.000	0.000	56.485
5	50.818	48.974	1.038	23.916	32.069	0.049	0.034	0.000	0.000	0.000	0.000	0.000	0.000	0.000	0.000	0.000	0.000	56.068
6	51.684	48.176	1.073	24.396	31.641	0.000	0.000	0.000	0.000	0.026	0.000	0.000	0.000	0.000	0.000	0.000	0.000	56.063
7	50.552	49.332	1.025	23.832	32.360	0.000	0.000	0.000	0.000	0.000	0.026	0.000	0.000	0.000	0.000	0.000	0.000	56.218
8	50.698	49.026	1.034	23.422	31.514	0.000	0.000	0.000	0.000	0.000	0.000	0.079	0.000	0.000	0.000	0.000	0.000	55.015
9	3.722	95.925	0.039	1.515	54.327	0.000	0.000	0.000	0.087	0.058	0.021	0.000	0.000	0.000	0.000	0.000	0.000	56.008
10	50.488	49.272	1.025	24.049	32.656	0.000	0.000	0.000	0.000	0.000	0.000	0.000	0.000	0.000	0.000	0.083	0.000	56.788
11	/	/	/	0.817	1.396	0.000	0.000	0.145	82.278	0.000	0.052	0.000	0.000	0.000	0.116	0.000	0.000	84.804
12	41.639	42.151	0.988	18.345	25.840	0.000	0.020	0.112	10.516	0.000	0.015	0.000	0.000	0.000	0.000	0.000	0.000	54.848
13	42.021	57.700	0.728	23.165	31.809	0.000	0.000	0.000	0.041	0.000	0.000	0.058	0.000	0.000	0.000	0.000	0.000	55.073
14	/	/	/	0.030	0.268	0.000	0.000	0.000	88.096	0.000	0.000	0.000	0.000	0.000	0.000	0.000	0.000	88.394
15	50.907	48.599	1.047	23.247	30.880	0.000	0.000	0.000	0.145	0.000	0.000	0.082	0.057	0.000	0.061	0.000	0.000	54.472
16	/	/	/	0.072	0.245	0.000	0.000	0.059	88.856	0.000	0.000	0.000	0.000	0.000	0.000	0.000	0.000	89.232
17	1.037	97.800	0.011	0.439	57.582	0.493	0.123	0.000	0.000	0.000	0.051	0.000	0.000	0.000	0.000	0.000	0.000	58.688
18	51.024	48.615	1.050	24.296	32.209	0.035	0.017	0.000	0.000	0.000	0.056	0.000	0.000	0.000	0.000	0.000	0.000	56.613

Table 3
Rare Earth Element of different types of dolomite ($\mu\text{g/g}$).

No.	Dolomite	Y	La	Ce	Pr	Nd	Sm	Eu	Gd	Tb	Dy	Ho	Er	Tm	Yb	Lu	ΣREE
YAB-1	D1	0.713	0.957	1.734	0.206	0.732	0.141	0.041	0.138	0.02	0.112	0.023	0.071	0.011	0.065	0.009	4.973
YAB-2	D1	0.773	0.958	1.993	0.219	0.782	0.153	0.031	0.147	0.02	0.131	0.024	0.077	0.011	0.078	0.01	5.407
YAB-3	D1	0.388	0.674	1.303	0.143	0.537	0.098	0.019	0.099	0.014	0.064	0.014	0.035	0.006	0.034	0.005	3.433
YAB-5	D1	0.546	0.685	1.392	0.144	0.559	0.102	0.021	0.111	0.015	0.086	0.018	0.05	0.006	0.038	0.005	3.778
YAB-6	D2	0.586	0.628	1.261	0.147	0.528	0.108	0.03	0.114	0.015	0.094	0.019	0.051	0.008	0.048	0.007	3.644
YAB-7	D2	0.935	0.921	1.858	0.196	0.763	0.148	0.032	0.153	0.022	0.139	0.026	0.075	0.011	0.059	0.008	5.346
YAB-8	D2	0.309	0.413	0.812	0.096	0.358	0.074	0.016	0.062	0.009	0.058	0.011	0.035	0.005	0.028	0.004	2.29
YAB-9	D2	0.335	0.35	0.708	0.083	0.302	0.057	0.014	0.06	0.009	0.053	0.011	0.037	0.005	0.03	0.004	2.058
YAB-10	D2	0.479	0.433	0.85	0.101	0.383	0.072	0.015	0.079	0.013	0.08	0.016	0.047	0.006	0.046	0.006	2.626
YAB-11	D2	0.351	0.423	0.831	0.097	0.335	0.068	0.015	0.072	0.009	0.06	0.012	0.03	0.005	0.026	0.004	2.338
YAB-12	D2	0.484	0.755	1.433	0.165	0.622	0.136	0.024	0.112	0.016	0.085	0.016	0.048	0.007	0.039	0.005	3.947
YAB-13	D3	0.498	0.678	1.393	0.149	0.542	0.108	0.032	0.111	0.014	0.085	0.017	0.045	0.006	0.046	0.006	3.73
YAB-14	D3	0.662	0.829	1.999	0.177	0.603	0.125	0.032	0.114	0.02	0.109	0.021	0.064	0.009	0.058	0.008	4.83
YAB-15	D3	0.839	1.098	2.665	0.309	1.233	0.236	0.048	0.204	0.021	0.14	0.029	0.088	0.011	0.073	0.011	7.005
YAB-16	D3	0.51	0.58	1.106	0.128	0.454	0.088	0.021	0.093	0.014	0.084	0.015	0.048	0.006	0.041	0.006	3.194
YAB-17	D3	0.483	0.476	0.861	0.104	0.374	0.074	0.016	0.078	0.015	0.083	0.014	0.04	0.005	0.037	0.005	2.665
YAB-18	D3	0.816	0.699	1.339	0.152	0.586	0.11	0.027	0.127	0.021	0.118	0.022	0.066	0.008	0.055	0.007	4.153
YAB-19	D3	0.301	0.501	0.97	0.104	0.389	0.084	0.015	0.074	0.009	0.056	0.011	0.036	0.005	0.031	0.004	2.59
YAB-20	D3	0.361	0.656	1.226	0.142	0.529	0.099	0.02	0.102	0.013	0.07	0.011	0.036	0.005	0.034	0.004	3.308
YAB-21	D3	0.546	1.488	2.792	0.297	1.131	0.167	0.03	0.16	0.019	0.092	0.018	0.051	0.007	0.047	0.007	6.852
YAB-22	D3	0.858	1.033	1.951	0.227	0.838	0.145	0.04	0.159	0.023	0.134	0.026	0.076	0.01	0.061	0.009	5.59
YAB-23	D3	0.363	0.683	1.422	0.153	0.548	0.102	0.023	0.1	0.012	0.07	0.012	0.039	0.005	0.032	0.004	3.568
YAB-24	D3	0.62	1.094	2.386	0.24	0.919	0.157	0.033	0.162	0.019	0.115	0.022	0.068	0.008	0.058	0.008	5.909
YAB-25	D3	0.497	1.142	1.513	0.171	0.618	0.12	0.024	0.121	0.016	0.087	0.017	0.048	0.007	0.044	0.007	4.432

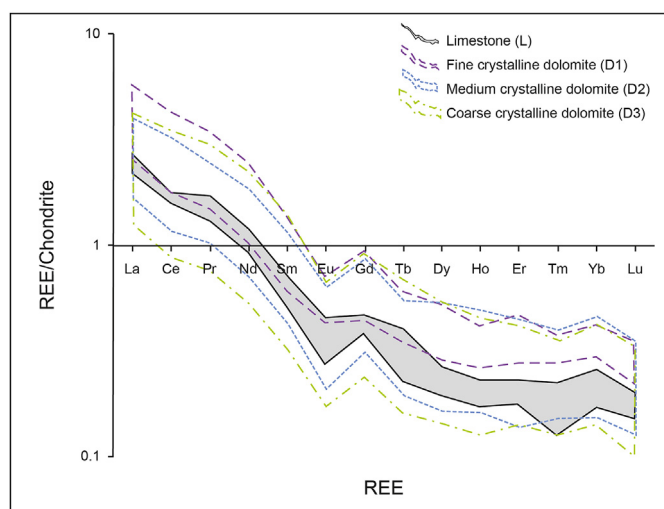


Fig. 10. Rare Earth Element patterns of different types of dolomite and limestone of Penglaiba Fm. in Yonganba Outcrop.

et al., 2011; Xing et al., 2011; Zhao et al., 2012). The increase in $^{87}\text{Sr}/^{86}\text{Sr}$ ratios with increasing depletion of $\delta^{18}\text{O}$ across most samples probably reveals the impact of hydrothermal activities, as do the two samples with abnormally depleted $\delta^{18}\text{O}$ values. However, we see no evidence indicating that the dolomite was modified significantly by hydrothermal fluids during or after dolomitization.

The REE composition of diagenetic carbonates is controlled by its precursors (e.g., Azmy et al., 2011) and reflected in the retention of their REE normalized pattern (Fig. 10). Thus, correlation of the REE compositions of dolomites with those of their precursor may shed light on the nature of the dolomitizing fluids (Azmy et al., 2013). The great similarity in ΣREE contents and pattern of D2 and D3 dolomites as well as limestone supports the interpretation of similar dolomitized fluid sources, i.e., dolomite inherited the REE from the limestone during burial dolomitization or the dolomitized fluids are seawater-derived fluids that limestone deposited from, as suggested by Zhang et al. (2008) and Zheng et al. (2013). In contrast,

relatively higher HREE compositions of D1 dolomite probably indicate different dolomitized fluids, which is consistent with the interpretation of penecontemporaneous dolomite based on the petrography observations.

5.3. Burial dolomitization: replacement or recrystallization

Geochemical data reveal the close relationships among the different dolomites, especially D2 and D3 dolomites; we take these relationships as evidence that the final states of dolomites probably formed by either replacement or recrystallization. However, petrographic data provide more detailed information on these rocks' dolomitization histories.

In the framing of Mazzullo's (1992) four criteria for recognizing altered dolomites, the Penglaiba Formation dolomites would present a complicated history. For D1 dolomite, little doubt exists regarding its formation and evolution. Petrographic and geochemical features tend to suggest penecontemporaneous dolomitization: the finely crystalline, fabric-retentive nature and dull cathodoluminescence, high Sr and low Mn concentrations, relatively high $\delta^{18}\text{O}$, late alteration or recrystallization according to the high ordering degree, slightly elevated $^{87}\text{Sr}/^{86}\text{Sr}$ ratios, and coarser dolomite crystals with clear rims. The main controversy lies in whether D2 and D3 dolomites are formed by direct replacement of grainstone to dolomite or by recrystallization of precursor dolomite.

The fact that D4 dolomite occurs between particles or along stylolites reveals that it is formed by direct replacement of grainstone. Additionally, patch-like D4 dolomites and D4 dolomites situated in intergranular areas occur in a single thin section (Fig. 8h, i) and show petrographic features and cathodoluminescence similar to those of D3 dolomite (Fig. 8j), showing that they share a common origin with D3 dolomite. D4 and D3 dolomites together provide a complete picture of replacive dolomite formed in burial environments. Dolomitizing fluids firstly moved through intergranular pores or stylolites and dolomitization occurred during shallow burial stage. Then, dolomite gradually replaced the grainstone, destroying fabrics including both particles and cements. Consequently, the grainstone texture was preserved in single D3 and D4

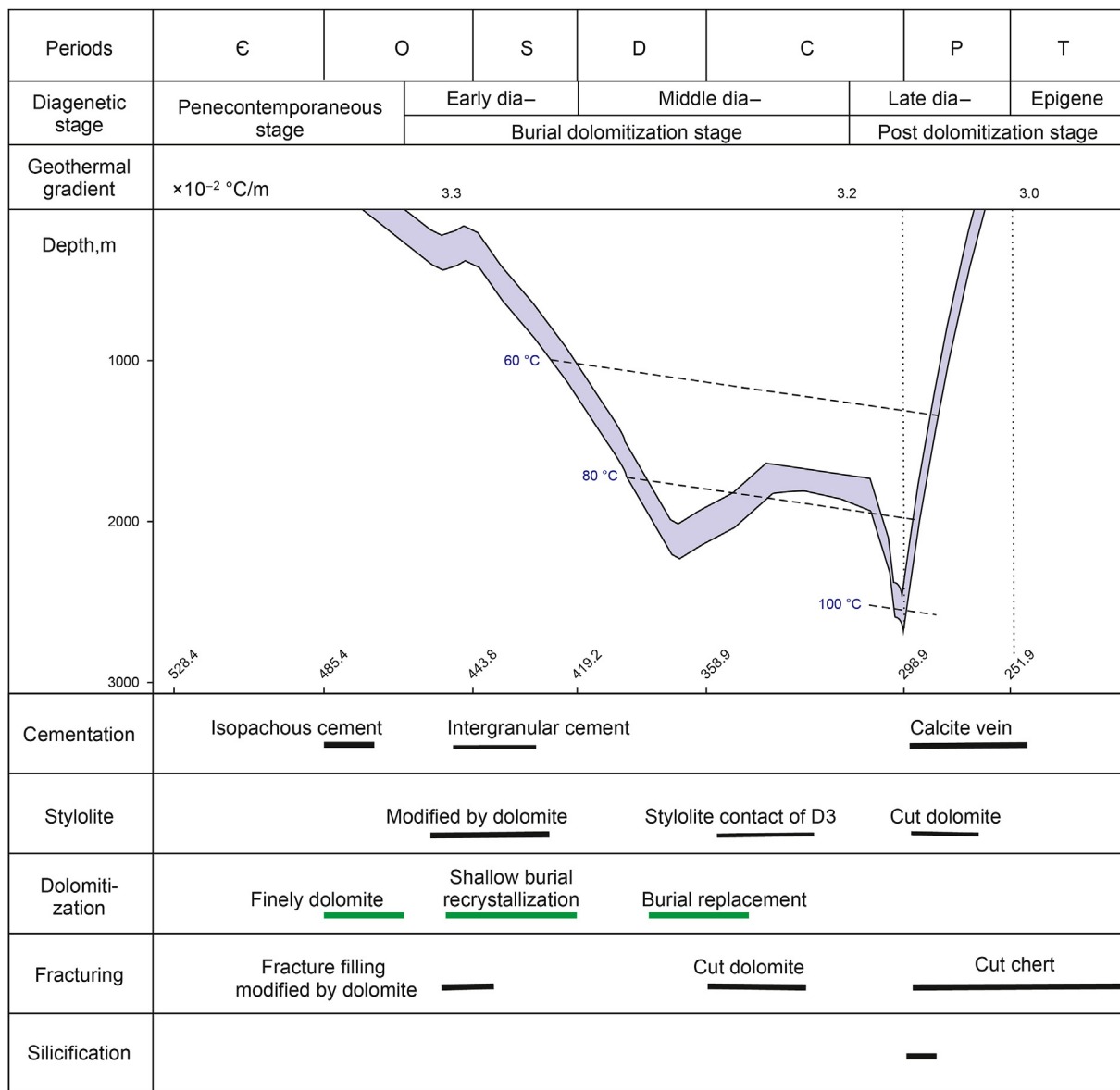


Fig. 11. Chart showing the paragenesis and dolomitization stages of Penglaiba Fm. of Yonganba Outcrop.

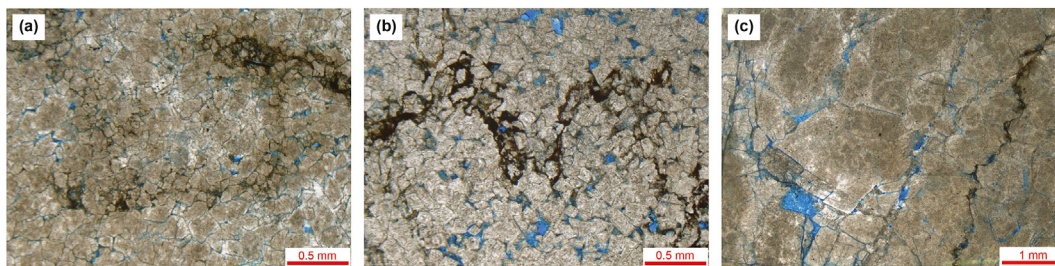


Fig. 12. Micrography images showing the relation of stylolite and dolomitization. (a) Micrograph showing stylolite modified by dolomitization with only ambiguous shape left; (b) Micrograph showing stylolite cut the D2 dolomite fabric, note that the incomplete dolomite crystals along the stylolite; (c) Micrograph showing stylolite cut the D3 dolomite.

dolomite crystals (Fig. 8h, i, and 14). Even though the dolomitization initiated in intergranular pores or stylolites, dolomitization was pervasive and fabric-destructive under the long history of burial and the influence of tectonic movement. This mechanism likely resulted in the seawater-derived geochemical characteristics

of Penglaiba Formation dolomite.

Compared to D1 dolomite, D2 dolomite is more stoichiometric (i.e., it has a higher ordering degree and is coarser in crystal size, with a planar texture, $\delta^{18}\text{O}$ and Sr depletion, and cloudy crystal centers surrounded by clear rims). All these features of D2 dolomite

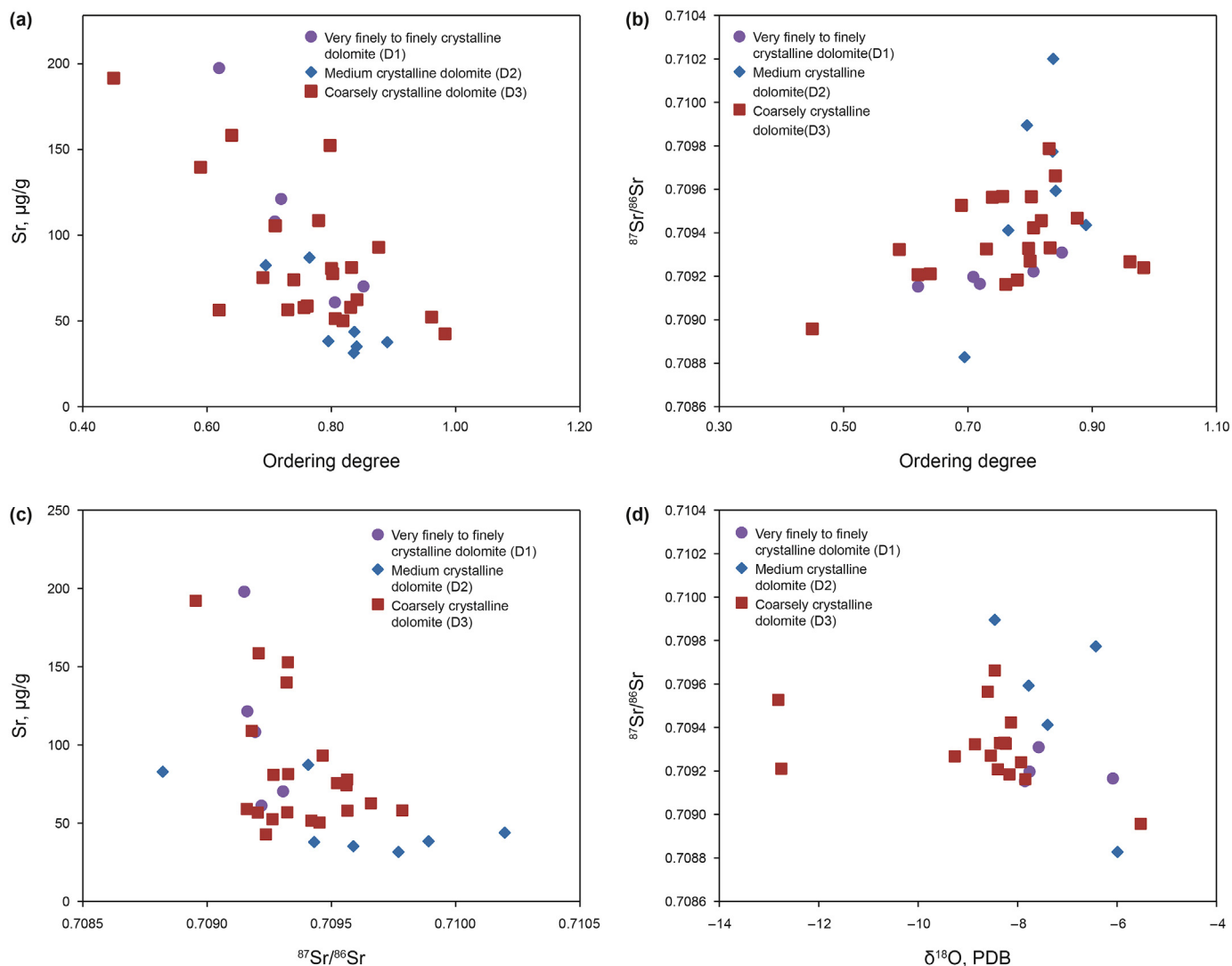


Fig. 13. Geochemistry of various Penglaiba Formation dolomites. **a** Relationship between the Sr content and dolomite ordering degree. **b** Relationship between the $^{87}\text{Sr}/^{86}\text{Sr}$ ratio and dolomite ordering degree. **c** Relationship between the Sr content and $^{87}\text{Sr}/^{86}\text{Sr}$ ratio. **d** Relationship between the $^{87}\text{Sr}/^{86}\text{Sr}$ ratio and $\delta^{18}\text{O}$.

comply with the criteria for recognizing the recrystallization of preexisting dolomite proposed by Mazzullo (1992). Additionally, thin section observations revealed that D2 dolomites tend to show ghosts of particles visible only when a white piece of paper is placed between the thin section and the light source, but only rarely appearing as fabric-retentive under normal microscope light transmission. Such evidence that the arrangement of D2 dolomite is strictly influenced by precursor textures supports the recrystallized dolomite hypothesis (Fig. 14), as in Kaczmarek and Sibley's (2011) contention that the initial dolomite phase provides a compositional template for future dolomite growth. Additionally, recrystallization is governed by heterogeneities in permeability, mineralogy, and corresponding reaction kinetics (Machel, 2004).

Medium- to coarsely crystalline dolomite crystals with a nonplanar and/or planar texture and a relatively narrow size distribution could result from the recrystallization of older, low-temperature dolomites (Sibley and Gregg, 1987; Gregg, 2004), like the Penglaiba Formation's D2 dolomite, in which case we should expect showing a close relationship to the precursor texture. However, D3 dolomitization was strongly fabric-destructive. The fact that D2 and D3 dolomites show similar geochemical trends

may indicate that they were formed or modified by the similar dolomitizing fluid. As Machel (2004) pointed out, if the fluids are hot and flow relatively quickly, and if they encounter highly porous preexisting dolostones, the latter may significantly recrystallize such that the resulting textures and geochemistry reflect the hot recrystallization event rather than the original dolomitization event. Meanwhile, the fluids also could cause the porous grainstone to be replaced by dolomite showing similar geochemical features. Thus, combination of the petrography with geochemistry suggests that D2 dolomite resulted from the recrystallization of preexisting dolomite (mostly like penecontemporaneous dolomite), whereas D3 dolomite formed by the replacement of precursor limestone. The different evolution routine of the dolomite caused the distinct petrography features and similar geochemical features.

To sum up, burial dolomitization includes both the recrystallization of preexisting dolomite and replacement of precursor limestone, and compared to the geochemistry features, the more important criteria to distinguish them would be the petrographic features, including: calcite inclusion, dolomite crystal structure, and the arrangement of dolomite crystals. The dolomite experienced the recrystallization tends to has less calcite inclusions,

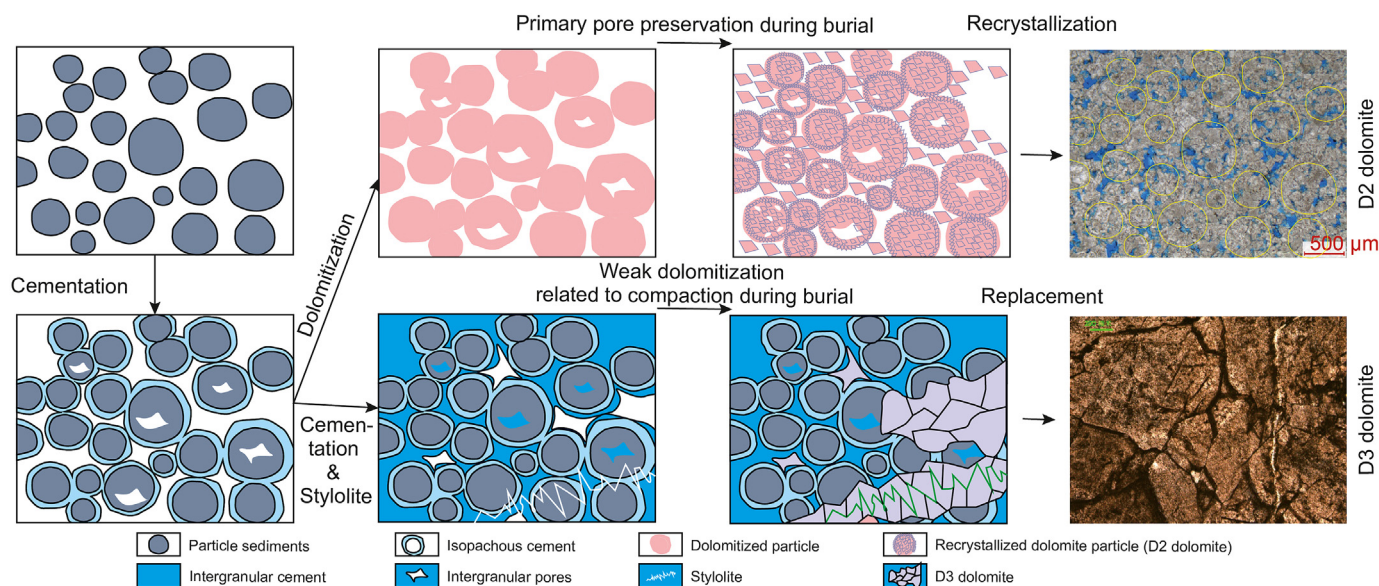


Fig. 14. Sketch showing the evolution routines of recrystallization of preexisting dolomite (D2 dolomite) and replacement of precursor limestone (D3 dolomite).

better ordered phases, and be arranged under the control of precursor fabric, whereas those formed by direct replacement of precursor limestone are inclined to be fabric-destructive, nonplanar texture, and less porosity. What's needed to point out is that the recrystallization of preexisting dolomite failed to show the homogenization of primary cathodoluminescent zonation as proposed by Mazzullo (1992), in contrast, the recrystallized dolomite shows obvious zonal features under cathodoluminescent.

One of remaining questions is why D2 dolomitized but D3 didn't before burial dolomitization. In spite of no direct evidence found, it is believed that it is attributed to the depositional and early stage diagenesis factors. Measured section revealed that Penglaiba Formation consists of lots of high frequency sequences composed of subtidal to intertidal cycles. In the framework of sequence stratigraphy, sediments in different part of sequences had distinct potential to the diagenesis. Those deposited in transgressive system tract tend to experience stronger cementation, whereas those in top part of cycles in the highstand system tract are inclined to experience stronger dissolution or penecontemporaneous dolomitization (Moore, 2001). Thin section analysis revealed that, even though both D2 and D3 are originally grainstone, D2 grainstone has apparently larger particle and better winnowed compared D3 grainstone (Fig. 7a,b and Fig. 8a,b), and more intragranular porosity in D2 suggested relatively stronger meteoric dissolution, in addition that the grainstones with D4 mostly are cemented tightly and situated in the vicinity of D3 dolomite and in the lower part of cycles indicate that D3 dolomite is the product between tightly cemented grainstone and D2 or D1 dolomite, controlled by the depositional sequence and early stage diagenesis.

5.4. Sources and transportation of massive dolomitized fluids

The formation of massive dolomite will definitely need massive dolomitized fluids, especially for the burial dolomite. As for the Penglaiba Formation in studied area, three sources of dolomitized fluids are believed contribute to the massive dolomite based on the geochemistry results and geological setting.

Firstly, the presence of D1 dolomite proves that sea water provided important Mg source for the penecontemporaneous dolomitization both for D1 and for precursor dolomite of D2, which is

consistent with the epeiric depositional environment characterized by subtidal–intertidal deposits during the Early Ordovician (Zhu and Ma, 1991). The open system during penecontemporaneous stage leaves no doubt on the Mg ion source and transportation.

Secondly, the seawater-derived pore fluids trapped in the formation played an important role on the shallow burial dolomitization. Hardie (1987) stated that Ca-rich waters may become dolomitizing fluids at temperatures above 60 °C according to the extrapolation from the high-temperature experiment data (275–400 °C), which would make most natural subsurface waters capable of dolomitization, even though dolomite has not been unequivocally synthesized in the laboratory under ambient conditions (Gregg et al., 2015). The burial history shows that Penglaiba Formation dolomite was buried to 600 m during the Late Ordovician to Silurian time and up to 1000 m during the Devonian time, with a corresponding temperature of up to 60 °C (Fig. 2). The observation that dolomites formed along with stylolites suggest burial of at least 600 m, as implied by the studies of Lind (1993) and Fabricius (2000). Development of nonplanar crystal textures and coarse planar textures also probably implies temperatures in excess of about 60 °C (Machel, 2004). At that point, the grainstone had undergone mineral stabilization to some extent but still preserved considerable porosity tended to be dolomitized. With the increasing burial depth and late Caledonian movement, the stabilization of carbonate and formation of stylolite would exclude considerable Mg ions and also cause the movement of formation fluids, consequently precursor dolomite recrystallized.

Thirdly, Penglaiba Formation rocks experienced regional uplift under the influence of thrusting during Hercynian tectonic movement, which probably pushed massive dolomitized fluids through the beds or penetrated the beds through faults, initiating the dolomitization phase. Even though the samples in this study failed to present obvious evidence of the fluids from other formation, it is very likely that the Cambrian dolomitized fluids transported and exerted an important role on the dolomitization, as mentioned by Cai et al. (2009) and Slater and Smith (2012).

In conclusion, for the widely distributed D3, it is important that they are interbedded with porous D2 dolomite and pervasive dolomitized fluid continuously flow in along the beds or faults due to regional compression. In another words, preserved porosities,

regional fluid flow, and relatively high temperatures led to pervasive dolomitization.

5.5. Implications for porosity development

The contribution of dolomitization to porosity is still controversial (Warren, 2000). Early models of porosity development in dolomite used the notions of volume reduction to explain sucrosic textures with high intercrystal porosity. That is to say, in a relatively closed system, the replacement of limestone (calcite or aragonite) by dolomite reduces the mineral volume, as dolomite has a smaller molar volume compared to either calcite or aragonite; therefore, dolomitization increases porosity (Murray, 1960; Weyl, 1960). In contrast, Lucia and Major (1994) pointed out that if there is an external source of carbonate and magnesium ions, then dolomitization of limestone typically results in a volume increase and a loss of total porosity. Indeed, no dolomite forms in a totally closed system, and external sources of carbonate and magnesium ions would be brought in during replacement and recrystallization in a burial environment. However, it is believed that the recrystallization of early formed dolomite tends to cause a different evolution of pores and porosity than the replacement of limestone by dolomite. D2 dolomite, formed by recrystallization of early dolomite, shows that the intercrystalline pores are closely related to the preexisting intergranular or intragranular pores (Fig. 7a, b), and host the highest quality reservoir (Fig. 15). We interpret the recrystallization as dramatically changing the shape and size of previously formed pores (Fig. 14), as mentioned by Gregg et al. (1993). D3 dolomite, formed by the replacement of limestone by dolomite, shows that vuggy pores and pores consisting mainly of fractures are rarely

related to the original fabric; this is consistent with the opinion of Lucia and Major (1994). However, the key differentiator is that D3 dolomite is probably easier to dissolve because of its more numerous calcite inclusions. As a result, more dissolved vugs typically formed in D3 dolomite, rather than intercrystalline pores. The differences in D2 and D3 dolomite crystal structure and evolution led in the burial stage to the differentiation of porosities (Fig. 14), which are crucial for Paleozoic dolomite in particular since it underwent longer and deeper burial compaction. Therefore, the important target for hydrocarbon exploration should be D2 dolomite (recrystallization of previously formed dolomite), which has a better chance of developing a substantial reservoir body. D2 is transformed from a previously or penecontemporaneously dolomitized porous body that tends to have higher compaction resistance and considerable primary porosity preserved during shallow burial, in this case, inner to middle ramp shoal would be favorable zone for the early dolomitization and preservation of porosity. In contrast, primary porosity can rarely be preserved in D3 dolomite because of the early cementation and pressure compaction during early shallow burial before dolomitization or replacement took place.

6. Conclusions

In the present work, we described the features and origins of dolomite of the Lower Ordovician Penglaiba Formation in the Tarim Basin, Northwest China, and discussed the implications of differences in recrystallization and replacement for dolomite origin and their influence on porosity development. The major findings of this study can be summarized as follows:

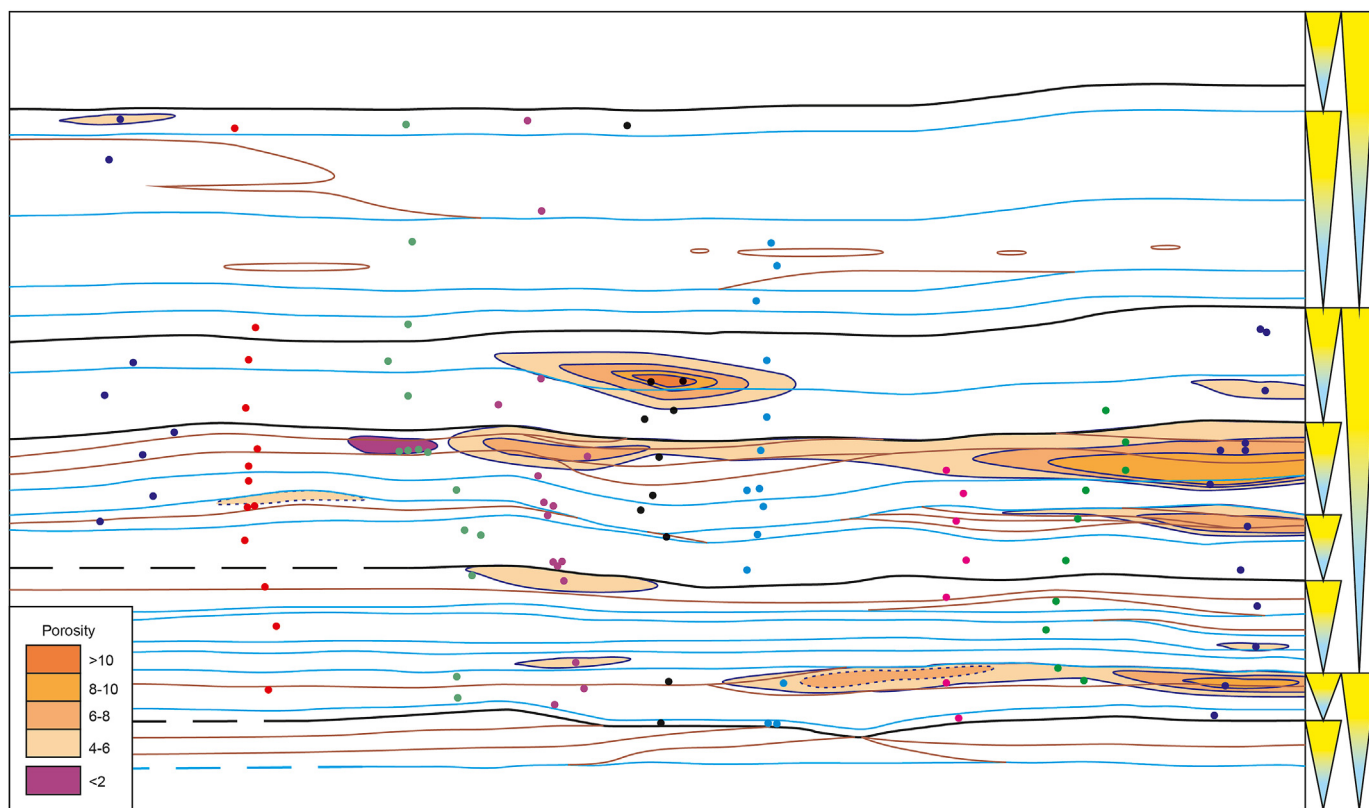


Fig. 15. Porosity isopachous chart of studied window showing the high porosity mainly distributed within the medium crystalline dolomite zone, where close to the sequence boundaries, the same area with Fig. 5a.

- (1) The Lower Ordovician Penglaiba Formation in the Yonganba outcrop trend of the Tarim Basin consists of three types of dolomite: very finely to finely crystalline nonplanar-a to planar-s dolomite (D1), medium-crystalline planar-s to planar-e dolomite (D2), and coarsely crystalline nonplanar-a dolomite (D3), all subject to burial dolomitization.
- (2) D1 and D2 dolomites are interpreted as dolomites that are formed before or during shallow burial and are later recrystallized. D3 is interpreted as dolomite formed by direct replacement of limestone during burial, probably by these same dolomitizing fluids, so that all three dolomites show similar geochemical features.
- (3) D2 dolomite, a dolomite recrystallized from a preexisting dolomite, tends to show more numerous intercrystalline pores (inherited from primary pores) and higher porosity owing to its outstanding compaction resistance during shallow burial. D3 dolomite tends to not develop considerable primary pores because of the strong cementation and pressure dissolution prior to dolomitization.

Acknowledgements

This study was supported by the National Science and Technology Major Projects of China (Grant No. 2016ZX05004002), PetroChina Science and Technology Project (Grant No. 2019B-0406) and the China Scholarship Council (No. 201908080005).

References

- Adams, J.E., Rhodes, M.L., 1960. Dolomitization by seepage refluxion. *AAPG Bull.* 44, 1912–1920.
- Al-Aasm, I.S., 2000. Chemical and isotopic constraints for recrystallization of sedimentary dolomites from the Western Canada sedimentary basin. *Aquat. Geochem.* 6, 227–248. <https://doi.org/10.1023/A:1009611224589>.
- Al-Aasm, I.S., Packard, J.J., 2000. Stabilization of early-formed dolomite: a tale of divergence from two Mississippian dolomites. *Sediment. Geol.* 131, 97–108. [https://doi.org/10.1016/S0037-0738\(99\)00132-3](https://doi.org/10.1016/S0037-0738(99)00132-3).
- Arvidson, R.S., Mackenzie, F.T., 1999. The dolomite problem; control of precipitation kinetics by temperature and saturation state. *Am. J. Sci.* 299 (4), 257–288. <https://doi.org/10.2475/ajs.299.4.257>.
- Azmy, K., Brand, U., Sylvester, P., Gleeson, S., Logan, A., Bitner, M.A., 2011. Biogenic low-Mg calcite (brachiopods): proxy of seawater-REE composition, natural processes and diagenetic alteration. *Chem. Geol.* 280, 180–190.
- Azmy, K., Lavoie, D., Wang, Z.R., Brand, U., Al-Aasm, I., Jackson, S., Girard, I., 2013. Magnesium-isotope and REE compositions of Lower Ordovician carbonates from eastern Laurentia: implications for the origin of dolomites and limestones. *Chem. Geol.* 356, 64–75. <https://doi.org/10.1016/j.chemgeo.2013.07.015>.
- Azmy, K., Veizer, J., Misi, A., Flávio de Oliveira, Tolentino, Sanches, A.L., Dardenne, M.A., 2001. Dolomitization and isotope stratigraphy of the vazante formation, são francisco basin, Brazil. *Precambrian Res.* 112 (3), 303–329. [https://doi.org/10.1016/S0301-9268\(01\)00194-2](https://doi.org/10.1016/S0301-9268(01)00194-2).
- Azomani, E., Azmy, K., Blamey, N., Brand, U., Al-Aasm, I., 2013. Origin of Lower Ordovician dolomites in eastern Laurentia: controls on porosity and implications from geochemistry. *Mar. Petrol. Geol.* 40, 99–114. <https://doi.org/10.1016/j.marpetgeo.2012.10.007>.
- Baadsgard, H., 1987. Rb-Sr and K-Ca isotope systematics in minerals from potassium horizons in the Prairie Evaporite Formation, Saskatchewan, Canada. *Chem. Geol. Isot. Geosci. Section.* 66, 1–15. [https://doi.org/10.1016/0168-9622\(87\)90022-4](https://doi.org/10.1016/0168-9622(87)90022-4).
- Baker, P.A., Burns, S.J., 1985. Occurrence and formation of dolomite in organic-rich continental margin sediments. *Bull. Am. Assoc. Petrol. Geol.* 69, 1917–1930.
- Banner, J.L., 1995. Application of the trace element and isotope geochemistry of strontium to studies of carbonate diagenesis. *Sedimentology* 42, 805–824. <https://doi.org/10.1111/j.1365-3091.1995.tb00410.x>.
- Budd, D.A., 1997. Cenozoic dolomites of carbonate islands: their attributes and origin. *Earth Sci. Rev.* 42, 1–47. [https://doi.org/10.1016/S0012-8252\(96\)00051-7](https://doi.org/10.1016/S0012-8252(96)00051-7).
- Cai, C.F., Hu, W.S., Worden, R.H., 2001. Thermochemical sulphate reduction in cambro-ordovician carbonates in central Tarim. *Mar. Petrol. Geol.* 18, 729–741.
- Cai, C.F., Li, K.K., Li, B., Cai, L., Jiang, L., 2009. Geochemical characteristics and origins of fracture- and vug-fillings of the Ordovician in Tahe oilfield, Tarim basin. *Acta Petrol. Sin.* 25 (10), 2399–2404.
- Carmichael, S.K., Ferry, J.M., 2008. Formation of replacement dolomite in the late-mar carbonate buildup, dolomites, northern Italy: part 2. origin of the dolomitizing fluid and the amount and duration of fluid flow. *Am. J. Sci.* 308 (8), 885–904. <https://doi.org/10.2475/08.2008.01>.
- Conliffe, J., Azmy, K., Greene, M., 2012. Dolomitization of the lower Ordovician Catoche formation: implications for hydrocarbon exploration in western Newfoundland. *Mar. Petrol. Geol.* 30, 161–173. <https://doi.org/10.1016/j.marpetgeo.2011.10.007>.
- Davies, G.R., Smith, L.B., 2006. Structurally controlled hydrothermal dolomite reservoir facies: an overview. *AAPG Bull.* 90, 1641–1690. <https://doi.org/10.1306/05220605164>.
- Ding, W.L., Qi, L.X., Yun, L., Yu, T., You, S., 2012. The tectonic evolution and its controlling effects on the development of Ordovician reservoir in Bachu-Markit Tarim basin. *Acta Petrol. Sin.* 28 (8), 2542–2556. <https://doi.org/10.3390/ijms141019618> (in Chinese).
- Dong, S., Chen, D., Zhou, X., Qian, Y.X., Qing, H.R., 2017. Tectonically driven dolomitization of Cambrian to Lower Ordovician carbonates of the Quruqtagh area, north-eastern flank of Tarim Basin, north-west China. *Sedimentology* 64 (4), 1079–1106. <https://doi.org/10.1111/sed.12341>.
- Eggs, S.M., Woodhead, J.D., Kinsley, L.P.J., Mortimer, G.E., Sylvester, P., McCulloch, M.T., Hergt, J.M., Handler, M.R., 1997. A simple method for the precise determination of ≥ 40 trace elements in geological samples by ICPMS using enriched isotope internal standardization. *Chem. Geol.* 134 (4), 311–326. [https://doi.org/10.1016/S0009-2541\(96\)00100-3](https://doi.org/10.1016/S0009-2541(96)00100-3).
- Fabricius, I.L., 2000. Interpretation of burial history and rebound from loading experiments and occurrence of microstylolites in mixed sediments of Caribbean Sites 999 and 1001. In: Leckie, R.M., Sigurdson, H., Acion, G.D., Draper, G. (Eds.), *Proceedings of the Ocean Drilling Program, Scientific Results*, 165. Ocean Drilling Program, College Station, TX.
- Folk, R.L., Land, L.S., 1975. Mg/Ca ratio and salinity: two controls on crystallization of dolomite. *Am. Assoc. Petrol. Geol. Bull.* 59, 60–68.
- Gao, Z.Q., Fan, T.L., Jiao, Z.F., Li, Y., 2006. The structural types and depositional characteristics of carbonate platform in the Cambrian-Ordovician of Tarim Basin. *Acta Sedimentol. Sin.* 24, 19–27. <https://doi.org/10.1007/s11442-006-0415-5> (in Chinese).
- Gregg, J.M., 2004. Basin fluid flow, base-metal sulphide mineralization and the development of dolomite petroleum reservoirs. In: Braithwaite, C.J.R., Rizzi, G., Darke, G. (Eds.), *The Geometry and Petrogenesis of Dolomite Hydrocarbon Reservoirs*, 235. Speical Publications, London, pp. 157–175. <https://doi.org/10.1144/GSL.SP.2004.235.01.07>. Geological Society.
- Gregg, J.M., Bish, D.L., Kaczmarek, S.E., Machel, H.G., Hollis, C., 2015. Mineralogy, nucleation and growth of dolomite in the laboratory and sedimentary environment: a review. *Sedimentology* 62 (6), 1749–1769. <https://doi.org/10.1111/sed.12202>.
- Gregg, J.M., Laudon, P.R., Woody, R.E., Shelton, K.L., 1993. Porosity evolution of the Cambrian Bonnetterre dolomite, south-eastern Missouri, USA. *Sedimentology* 40, 1153–1169. <https://doi.org/10.1111/j.1365-3091.1993.tb01385.x>.
- Gregg, J.M., Shelton, K.L., 1990. Dolomitization and dolomite neomorphism in the back reef facies of the Bonnetterre and Davis formations (Cambrian), south-eastern Missouri. *J. Sediment. Petrol.* 60, 549–562. <https://doi.org/10.1306/212F91E2-2B24-11D7-8648000102C1865D>.
- Gu, J.Y., 2000. The feature and origin of lower Ordovician dolomite in Tarim basin. *Xinjing Pet. Geol.* 21 (2), 120–122 (in Chinese).
- Guo, C., Chen, D., Qing, H., Dong, S.F., Li, G., Wang, D., Qian, Y., Liu, C., 2016. Multiple dolomitization and later hydrothermal alteration on the Upper Cambrian-Lower Ordovician carbonates in the northern Tarim Basin, China. *Mar. Petrol. Geol.* 72, 295–316. <https://doi.org/10.1016/j.marpetgeo.2016.01.023>.
- Hardie, L.A., 1987. Dolomitization: a critical view of some current views. *J. Sediment. Petrol.* 57, 166–183. <https://doi.org/10.1306/212F8AD5-2B24-11D7-8648000102C1865D>.
- Hu, M.Y., Jia, Z.Y., 1991. The origin of Xiaqiluitaga Graoup dolomite in Keping area, Tarim basin. *Journal of Jiangnan Petroleum Institute* 13 (2), 10–17 (in Chinese).
- Hu, M.Y., 1993. Diagenesis and porosity evolution of Cambrian carbonate rock in the north Tarim Basin. *Journal of Jiangnan Petroleum Institute* 2, 1–8 (in Chinese).
- Huang, S.J., Qing, H., Pei, C.R., Hu, Z.W., Wu, S.J., Sun, Z.L., 2006. Strontium concentration, isotope composition and dolomitization fluids in the Feixianguan Formation of triassic, eastern sichuan of China. *Acta Petrol. Sin.* 22 (8), 2123–2132. <https://doi.org/10.2113/gssaj.109.3.411> (in Chinese).
- Jiao, C.L., He, Z.L., Xing, X.J., Qing, H.R., He, B.Z., Li, C.C., 2011. Tectonic hydrothermal dolomite and its significance of reservoirs in Tarim basin. *Acta Petrol. Sin.* 27 (1), 277–284. <https://doi.org/10.1134/S002449021101007X>.
- Kaczmarek, S.E., Sibley, D.F., 2011. On the evolution of dolomite stoichiometry and cation order during high-temperature synthesis experiments: an alternative model for the geochemical evolution of natural dolomites. *Sediment. Geol.* 240 (1), 30–40. <https://doi.org/10.1016/j.sedgeo.2011.07.003>.
- Kamber, B.S., Greig, A., Schoenberg, R., Collerson, K.D., 2003. A refined solution to Earth's hidden niobium: implications for evolution of continental crust and mode of core formation. *Precambrian Res.* 126 (3–4), 289–308. [https://doi.org/10.1016/S0301-9268\(03\)00100-1](https://doi.org/10.1016/S0301-9268(03)00100-1).
- Kang, Y.Z., Kang, Z.H., 1994. Tectonic evolution and oil and gas of Tarim Basin. *Acta Geosci. Sin.* 3 (4), 180–191. [https://doi.org/10.1016/0743-9547\(96\)00038-4](https://doi.org/10.1016/0743-9547(96)00038-4) (in Chinese).
- Kimbell, T.N., Humphrey, J.D., 1994. Geochemistry and crystal morphology of aragonite cements of mixing-zone origin, Barbados, West Indies. *J. Sediment. Res.* A64, 604–614. <https://doi.org/10.1111/j.1525-1314.1994.tb00042.x>.
- Land, L.S., 1980. The isotopic and trace element geochemistry of dolomite: the state of the art. In: Zenger, D.H., Dunham, J.B., Ethington, R.L. (Eds.), *Concepts and Models of Dolomitization*, 28. SEPM Special Publication, pp. 87–110.
- Land, L.S., 1985. The origin of massive dolomite. *J. Geol. Educ.* 33, 112–125.
- Lapponi, F., Bechstadt, T., Boni, M., Banks, D.A., Schneider, J., Immenhauser, A., 2014. Hydrothermal dolomitization in a complex geodynamic setting (lower

- palaeozoic, northern Spain). *Sedimentology* 61 (2), 1–33. <https://doi.org/10.1111/sed.12060>.
- Li, B.P., Greig, A., Zhao, J.X., Collerson, K.D., Quan, K.S., Meng, Y.H., Ma, Z.L., 2005. ICP-MS trace element analysis of Song dynasty porcelains from Ding, Jiexiu and Guantai kilns, north China. *J. Archaeol. Sci.* 32 (2), 251–259. <https://doi.org/10.1016/j.jas.2004.09.004>.
- Lind, L.L., 1993. Stylolites in chalk from leg 130, ontong java plateau. In: Berger, W.H., Kroenke, J.W., Mayer, L.A. (Eds.), *Proceedings of the Ocean Drilling Program, Scientific Results, 130*. Ocean Drilling Program, College Station, TX. <https://doi.org/10.2973/odp.proc.sr.130.006.1993>.
- Lucia, F.J., Major, R.P., 1994. Porosity evolution through hypersaline reflux dolomitization. In: Purser, B., Tucker, M., Zenger, D. (Eds.), *Dolomites-A Volume in Honor of Dolomieu*, 21. Spec. Publ. Int. Assoc. Sedimentol., pp. 325–341.
- Machel, H.G., 2004. Concepts and models of dolomitization: a critical reappraisal. In: Braithwaite, C.J.R., Rizzi, G., Darke, G. (Eds.), *Oirs*, the Geological Society of London, The Geometry and Petrogenesis of Dolomite Hydrocarbon Reserv., 235. Special Publication, pp. 7–63. <https://doi.org/10.1144/GSL.SP.2004.235.01.02>.
- Malone, M.J., Baker, P.A., Burns, S.J., 2010. Recrystallization of dolomite: evidence from the Monterey Formation (Miocene), California. *Sedimentology* 41 (6), 1223–1239. <https://doi.org/10.1111/j.1365-3091.1994.tb01450.x>.
- Mazzullo, S.J., 1992. Geochemical and neomorphic alteration of dolomite: a review. *Carbonates Evaporites* 6, 21–37. <https://doi.org/10.1007/BF03175390>.
- Montanez, I.P., Read, J.F., 1991. Fluid-rock interaction history during stabilization of early dolomites, upper Knox Group (Lower Ordovician), U.S. Appalachians. *J. Sediment. Petrol.* 62 (5), 753–778. <https://doi.org/10.1306/D42679D3-2B26-11D7-8648000102C1865D>.
- Moore, C., 2001. *Carbonate Reservoirs: Porosity, Evolution and Diagenesis in a Sequence Stratigraphic Framework*. Elsevier Science.
- Morrow, D.W., 1982. Diagenesis 2. Dolomite: Part 2. Dolomitization models and ancient dolostones. *Geosci. Can.* 9, 95–107. <https://doi.org/10.12789/gsc.v9i2.3299>.
- Murray, R.C., 1960. Origin of porosity in carbonate rocks. *J. Sediment. Petrol.* 30, 59–84. <https://doi.org/10.1306/74D709CA-2B21-11D7-8648000102C1865D>.
- Pan, L.Y., Shen, A.J., Shou, J.F., Hu, A.P., Wei, D.X., 2016. Fluid inclusion and geochemical evidence for the origin of sparry calcite cements in Upper Permian Changxing reefal limestones, eastern Sichuan Basin (SW China). *J. Geochem. Explor.* 171, 124–132. <https://doi.org/10.1016/j.gexplo.2016.01.006>.
- Qian, Y.X., You, D.H., 2006. An analysis of ordovician dolomitisation origin in northwestern tazhong area. *Xinjing Pet. Geol.* 27 (2), 146–150. <https://doi.org/10.1360/aps050121>.
- Qiao, Z.F., Shen, A.J., Zheng, J.F., Hu, J., Wu, X.N., Lu, J.M., 2012. Classification and origin of the lower ordovician dolostone in Tarim Basin. *J. Palaeogeogr.* 14 (1), 21–32. <https://doi.org/10.1007/s11783-011-0280-z> (in Chinese).
- Qing, H.R., Bosence, D.W., Rose, E.P., 2001. Dolomitization by penesaline sea water in Early Jurassic peritidal platform carbonates, Gibraltar, western Mediterranean. *Sedimentology* 48, 153–163. <https://doi.org/10.1046/j.1365-3091.2001.00361.x>.
- Qing, H.R., Veizer, J., 1994. Oxygen and carbon isotopic composition of Ordovician brachiopods: implications for coeval seawater. *Geochem. Cosmochim. Acta* 58, 4429–4442.
- Qing, H.R., Barnes, C.R., Buhl, D., Veizer, J., 1998. The Strontium isotopic composition of Ordovician and Silurian brachiopods and conodonts: relationships to geological events and implications for coeval seawater. *Geochem. Cosmochim. Acta* 62, 1721–1734. [https://doi.org/10.1016/S0016-7037\(98\)00104-5](https://doi.org/10.1016/S0016-7037(98)00104-5).
- Reinhold, C., 1998. Multiple episodes of dolomitization and dolomite recrystallization during shallow burial in Upper Jurassic shelf carbonates: eastern Swabian Alb, southern Germany. *Sediment. Geol.* 121 (1–2), 71–95. [https://doi.org/10.1016/S0037-0738\(98\)00077-3](https://doi.org/10.1016/S0037-0738(98)00077-3).
- Ronchi, P., Jadoul, F., Ceriani, A., Di Giulio, A., Scotti, P., Ortenzi, A., Previde Massara, E., 2011. Multistage dolomitization and distribution of dolomitized bodies in Early Jurassic carbonate platforms (Southern Alps, Italy). *Sedimentology* 58, 532–565.
- Rott, C.M., Qing, H.R., 2013. Early dolomitization and recrystallization in shallow marine carbonates, Mississippian Alida beds, Williston Basin (Canada): evidence from petrography and isotope geochemistry. *J. Sediment. Res.* 83, 928–941. <https://doi.org/10.2110/jsr.2013.73>.
- Shao, L.Y., He, H., Peng, S.P., 2002. The types and origin of dolostones of the Cambrian and Ordovician in Bachu uplift area of Tarim basin. *J. Palaeogeogr.* 4 (2), 19–28. <https://doi.org/10.1080/12265080208422884> (in Chinese).
- Shields, G.A., Carden, G.A., Veizer, J., Meidla, T., Rong, J.Y., Li, R.Y., Sr, C., 2003. O isotope geochemistry of Ordovician brachiopods: a major isotopic event around the Middle-Late Ordovician transition. *Geochem. Cosmochim. Acta* 67, 2005–2025. [https://doi.org/10.1016/S0016-7037\(02\)01116-X](https://doi.org/10.1016/S0016-7037(02)01116-X).
- Sibley, D.F., Gregg, J.M., 1987. Classification of dolomite rock textures. *J. Sediment. Petrol.* 57, 967–975. <https://doi.org/10.1306/212F8CBA-2B24-11D7-8648000102C1865D>.
- Slater, B.E., Smith Jr., L.B., 2012. Outcrop analog for trenton-black river hydrothermal dolomite reservoirs, mohawk valley, New York. AAPG (Am. Assoc. Pet. Geol.) Bull. 96 (7), 1369–1388. <https://doi.org/10.1306/100411102000>.
- Sun, S.Q., 1994. A reappraisal of dolomite abundance and occurrence in the Phanerozoic: perspective. *J. Sediment. Res.* A64, 396–404. <https://doi.org/10.1306/D426808B-2B26-11D7-8648000102C1865D>.
- Sun, L.H., Wang, Y.J., Fan, W.M., Peng, T.P., 2007. Petrogenesis and tectonic significances of the diabase dikes in the Bachu area, Xinjiang. *Acta Petrol. Sin.* 23 (6), 1369–1380. <https://doi.org/10.1016/j.sedgeo.2005.09.025> (in Chinese).
- Tucker, M.E., Wright, V.P., 1990. *Carbonate Sedimentology*. Blackwell Scientific Publication, Oxford.
- Veizer, J., Ala, D., Azmy, K., Bruckschen, P., 1999. $^{87}\text{Sr}/^{86}\text{Sr}$, $\delta^{13}\text{C}$ and $\delta^{18}\text{O}$ evolution of Phanerozoic seawater. *Chem. Geol.* 161, 59–88. [https://doi.org/10.1016/S0009-2541\(99\)00081-9](https://doi.org/10.1016/S0009-2541(99)00081-9).
- Vahrenkamp, V.C., Swart, P.K., 1990. New distribution coefficient for the incorporation of strontium into dolomite and its implications for the formation of ancient dolomites. *Geology* 18, 387–391. [https://doi.org/10.1130/0091-7613\(1990\)0182.3.CO;2](https://doi.org/10.1130/0091-7613(1990)0182.3.CO;2).
- Wadleigh, M.A., Veizer, J., 1992. $^{18}\text{O}/^{16}\text{O}$ and $^{13}\text{C}/^{12}\text{C}$ in Lower Paleozoic articulate brachiopods: implications for the isotopic composition seawater. *Geochem. Cosmochim. Acta* 56, 431–443. [https://doi.org/10.1016/0016-7037\(92\)90143-7](https://doi.org/10.1016/0016-7037(92)90143-7).
- Warren, J., 2000. Dolomite: occurrence, evolution and economically important association. *Earth Sci. Rev.* 52, 1–81. [https://doi.org/10.1016/S0012-8252\(00\)00022-2](https://doi.org/10.1016/S0012-8252(00)00022-2).
- Weyl, P.K., 1960. Porosity through dolomitization: conservation of mass requirements. *J. Sediment. Petrol.* 30, 85–90. <https://doi.org/10.1306/74D709CF-2B21-11D7-8648000102C1865D>.
- Wierzbicki, R., Dravis, J.J., Alaasm, I., Harland, N., 2006. Burial dolomitization and dissolution of upper jurassic Abenaki platform carbonates, deep panuke reservoir, nova scotia, Canada. AAPG Bull. 90 (11), 1843–1861. <https://doi.org/10.1306/03200605074>.
- Wu, S.Q., Zhu, J.Q., Wang, G.X., Hu, W.X., Zhang, J.T., Wang, X.L., 2008. Types and origin of Cambrian-Ordovician dolomites in Tarim basin. *Acta Petrol. Sin.* 24 (6), 1390–1400 (in Chinese).
- Xing, F.C., Zhang, W.H., Li, S.T., 2011. Influence of hot fluids on reservoir property of deep buried dolomite and its significance for petroleum exploration: a case study of Keping outcrop in Tarim basin. *Acta Petrol. Sin.* 27 (1), 266–276. <https://doi.org/10.1007/s11769-011-0445-5> (in Chinese).
- Yang, W., Wang, Q.H., Liu, X.Z., 2000. Dolomite origin of lower ordovician in hetian river gas field, Tarim Basin. *Acta Sedimentol. Sin.* 18 (4), 544–547 (in Chinese).
- Yu, B.S., Chen, J.Q., Lin, C.S., 2001. Sequence stratigraphy of Cambrian-Ordovician successions of northern Tarim Basin and its correlation with those of Yangtze and north China platforms. *Sci. China Earth Sci.* 31, 17–26. <https://doi.org/10.3969/j.issn.1674-7313.2001.04.010> (in Chinese).
- Zhang, X.F., Hu, W.X., Zhang, J.T., Wang, X.L., Xie, X.M., 2008. Geochemical analyses on dolomitizing fluids of Lower Ordovician carbonate reservoir in Tarim basin. *Earth Sci. Front.* 15 (2), 80–89. [https://doi.org/10.1016/S1872-5791\(08\)60018-4](https://doi.org/10.1016/S1872-5791(08)60018-4) (in Chinese).
- Zhang, J., Luo, P., 2010. Genesis of ordovician matrix-porosity dolomite reservoir in the Tarim Basin. *Petroleum Geology & Experiment* 32 (5), 470–474. [https://doi.org/10.1016/S1876-3804\(11\)60008-6](https://doi.org/10.1016/S1876-3804(11)60008-6), 503.
- Zhang, C., Zheng, D.M., Li, J.H., 2001. Attribute of paleozoic structures and its evolution characteristics in Keping fault-uplift. *Oil Gas Geol.* 22 (4), 314–318. <https://doi.org/10.11743/ogg20010406> (in Chinese).
- Zhao, W.Z., Shen, A.J., Hu, S.Y., Pan, W.Q., Zheng, J.F., Qiao, Z.F., 2012. Types and distributional features of Cambrian-Ordovician dolostone reservoirs in Tarim basin, northwestern China. *Acta Petrol. Sin.* 28 (3), 758–768. <https://doi.org/10.2110/palo.2011.p11-036r> (in Chinese).
- Zheng, J.F., Shen, A.J., Qiao, Z.F., Ni, X.F., 2013. Genesis of dolomite and main controlling factors of reservoir in Penglaiba Formation of Lower Ordovician, Tarim Basin: a case study of Dabantage outcrop in Bachu area. *Acta Petrol. Sin.* 29 (9), 3223–3232. <https://doi.org/10.1086/671395>.
- Zheng, H.R., Wu, M.B., Wu, X.W., Zhang, T., Liu, C.Y., 2007. Oil-gas exploration prospect of dolomite reservoir in the lower paleozoic of Tarim Basin. *Acta Pet. Sin.* 28 (2), 1–8. <https://doi.org/10.3321/j.issn:0253-2697.2007.02.001> (in Chinese).
- Zhu, D.Y., Jin, Z.J., Hu, W.X., 2009. Hydrothermal alteration dolomite reservoir in Tazhong area. *Acta Pet. Sin.* 30 (5), 698–704. <https://doi.org/10.7623/syxb200905011>.
- Zhu, D.Y., Jin, Z.J., Hu, W.X., 2010. Hydrothermal recrystallization of the Lower Ordovician dolomite and its significance to reservoir in northern Tarim Basin. *Sci. China Earth Sci.* 51 (3), 140. <https://doi.org/10.1007/s11430.010-0028>.
- Zhu, L.F., Ma, B.L., 1991. The sedimentary environment of cambrian-ordovician in the Aksu and keping areas of Tarim Basin. *Acta Sedimentol. Sin.* 9 (2), 55–62 (in Chinese).
- Zhu, J.Q., Wu, S.Q., Wang, G.X., Hu, W.X., 2008. Types and porosity characteristics of the Cambrian-Ordovician dolostones in Tarim basin. *Earth Sci. Front.* 15 (2), 67–79 (in Chinese).